NASA TECHNICAL MEMORANDUM NASA TM-77552

DIRECTIONAL SOLIDIFICATION OF Al_2-Cu-Al AND Al_3-Ni-Al EUTECTICS DURING TEXUS ROCKET FLIGHT

J.J. Favier, J. de Goer

Translation of D.M.G. Report No. 93/83,
Centre d'Etudes Nucleaires de Grenoble,
Department de Metallurgie de Grenoble,
Grenoble, France, November 1983,
pp 1 - 56

NATIONAL AERONAUTICS AND SPACE ADMINISTRATION
WASHINGTON D.C. 20546 JUNE 1984

STANDARD TITLE PAGE

1. Report No. NASA TM-77552	2. Government Accession No.	3. Recipient's Catalog No.
4. Title and Subtitle DIRECTIONAL SOLIDIFICATION OF Al_2Cu-Al AND Al_3Ni-Al EUTECTICS DURING TEXUS ROCKET FLIGHT		5. Report Date JUNE 1984 6. Performing Organization Code
7. Author(s) J.J. Favier, J. de Goer		8. Performing Organization Report No. 10. Work Unit No.
9. Performing Organization Name and Address SCITRAN Box 5456 Santa Barbara, CA 93108		11. Contract or Grant No. NASw 3542 13. Type of Report and Period Covered Translation
12. Sponsoring Agency Name and Address National Aeronautics and Space Administration Washington, D.C. 20546		14. Sponsoring Agency Code

15. Supplementary Notes

Translation of D.M. G. Report No. 93/83. Centre d'Etudes Nucleaires de Grenoble, Department de Metallurgie de Grenoble, Grenoble, France, November 1983, pp 1 - 56.

16. Abstract

One lamellar eutectic sample and one fiber-like eutectic sample were solidified directionally during the TEXUS VI rocket flight of 8 May 1982. The microstructures and the results of the thermal analysis, obtained from the temperatures recorded on the cartridge skin, are compared. It is found that no appreciable modifications of the regularity of the eutectic structures were observed by passing from 1 g to 10^{-4} g in these experiments. No steady state growth conditions were achieved in these experiments.

17. Key Words (Selected by Author(s))	18. Distribution Statement
	Unclassified and Unlimited

19. Security Classif. (of this report)	20. Security Classif. (of this page)	21. No. of Pages	22. Price
Unclassified	Unclassified	60	

ABSTRACT

One lamellar eutectic sample (Al_2Cu-Al) and one fiber-like eutectic sample (Al_3Ni-Al) were solidified directionally during the TEXUS VI rocket flight of May 8, 1982.

The structures were carefully studied and the lamellar or fibrous spacings (λ) were measured by laser diffraction along the full samples.

*Al_2Cu-Al eutectic:

A comparison between the microstructures and the results of the thermal analysis deduced from the temperatures recorded on the cartridge skin indicates that:

-The law of variation between λ and the interface velocity V takes the same $\lambda^2 V = k$ form under 10^{-4} and 1 g.

-The g level does not modify the value of the k constant, $k = 8.8 \cdot 10^{-11}$ CGS.

*Al_3Ni-Al eutectic:

An important perturbation of the solidification process at the launch (backmelting of more than 7 mm of sample) does not permit a categorical conclusion.

However, if an eventual effect of the microgravity level can be estimated, it seems to increase the fiber spacing. This is in contradiction with the observations by Pirich and Larson on the Mn-Bi eutectic solidified in the SPAR program.

No appreciable modifications of the regularity of the eutectic structures were observed by passing from 1 g to 10^{-4} g in these experiments, contrary to the results by Hasenmeyer on the Al_2Cu-Al

eutectic during the Skylab mission. It must be mentioned, however, that no steady state growth conditions were achieved in these experiments, due to the nonsteady thermal conditions (V increases) and the rapid morphological destabilization of the solidification front after a few tens of seconds of microgravity conditions. The nearest experiments in the Spacelab on the same systems should permit a better approach to this last point.

TABLE OF CONTENTS

TABLE OF CONTENTS (continued)

I - INTRODUCTION /2*

A binary alloy of one-directional solidified eutectic composition (on the front plane) generally exhibits an organized anistropic structure:

-lamellar stacking of two phases of defined compositions (case of Al_2Cu-Al),

-fiber cluster of one phase in the matrix of another phase (case of Al_3Ni-Al).

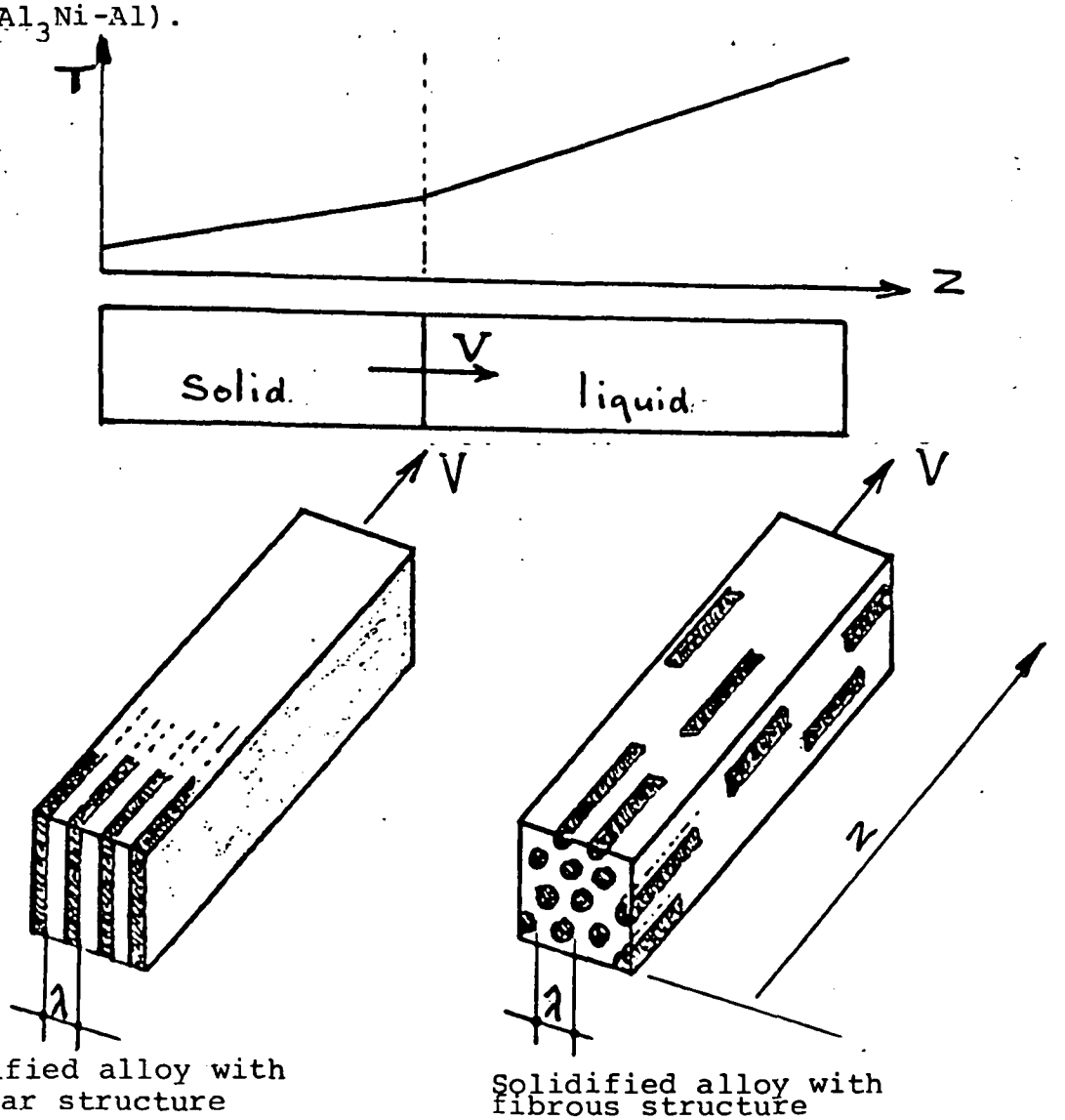

Figure 1

*Numbers in the margin indicate pagination in the original text.

A relationship expressed as $\lambda^2 V = k$ between the rate of displacement of the solidification front and "cycle" λ of the lamellar or fibrous microstructure of the solidified alloy was experimentally demonstrated in numerous systems [1], and was theoretically explained using conventional coupled eutectic solidification models [2]. /3

In the case of alloys solidified at the ground, numerical values of the constant may be deduced from publications of various authors,

Alloy	Structure	$k = \lambda^2 V$ (λ in µm) (V in cm·h^{-1})	Reference
Al_2Cu-Al	Lamellar	31.6	[1]
Al_3Ni-Al	Fibrous	25	[2]

Pirich and Larson performed two space directed solidification experiments of fibrous Bi-MnBi eutectic during the SPAR rocket-probe flights [13]. These authors found that the fiber diameter and the inter-fiber spacing at the time of solidification in microgravity were 70% and 65 %, respectively, of their ground values, in solidification conditions considered to be identical.

Finally, Hasenmeyer considered studying the regularity of the eutectic structures in his American experiment performed on board the Skylab [4]. Although the conditions of the space experiment were never specified, this author affirms that he observed an improvement in the structures perfected by about 20%, /4 which is not significant, if we consider the uncertainties

in the quantification.

The objective of these rocket-probe experiments on regular eutectics is two-fold:

-first, like the experiments conducted simultaneously on doped germanium, we want to prove : the feasibility of a directional solidification experiment, in microgravity conditions, aboard a rocket-probe. Its interest is that it is cheaper than an experiment on board an orbital station and it is flexible to use.

-we are also trying to answer the following questions concerning the mechanisms of regular eutectic solidification:

-Is the law $\lambda^2 V = Cste$ still verified in space? Is the constant different for 1 g and in microgravity? This seems to be the case for the Mn-Bi system.

-Is the regularity of the eutectic structure affected by the gravity level? Use of an objective analysis and measuring technique is required, and we developed a specific method using laser diffraction.

More precise elements in the answer to these questions will certainly be obtained during the F.S.L.P experiments on these same alloys, for which these TEXUS IV and TEXUS VI rocket-probe programs are only a preliminary phase.

This report first describes the techniques of analyzing the thermal data obtained from continuous temperature recordings on the cartridge and in the oven. From this, we deduce the solidification rates and thermal gradients. Then, we describe the metallographic characterization of the structures obtained. Finally, for both eutectic systems, we try to correlate the growth and structural conditions, which are essentially rate and eutectic period on the one hand and gravity level and structural regularity on the other hand.

II - DEVICE AND EXPERIMENTAL CONDITIONS

Only very small modifications were made versus the earlier experiment performed during the TEXUS VI flight and discussed in reference [5].

II.1. Modification at the cartridge level:

As announced in [5], the length in the charge was reduced to 70 mm (figure 1). In the space thus liberated, we lodged a boron nitride piston activated by stacked rings made of elastic graphite felt. The function of this system is to slightly compress the liquefied charge to avoid vacuum formation during solidification.

II.2 Modifications at the thermal cycles level:

Newly defined for Al-Ni, and refined for Al-Cu, they should make it possible:

-to retain for solidification an initial 20 to 25 mm seed, resulting in the positioning of the resolidified part in a thermically favorable region (region without radial gradient, in which the front is flat),

-to obtain the required solidified length on the ground (5 to 10 mm) and a solidified length in microgravity of 5 to 10 mm as well, while the solification rate should remain moderate to prevent destabilization of the interface ($V < 7$ cm/j).

II.3 Sample identification /6

FLIGHT	MODULUS	FURNACE	ALLOY	CHARGE REF.
TEXUS IV	TEM 03	A	Al_2Cu-Al	024
TEXUS VI	TEM 03	B	Al_2Cu-Al	032
TEXUS VI	TEM 03	A	Al_3Ni-Al	026

II.4 Conditions specific to the TEXUS VI flight:

The ballistic and thermal conditions were virtually nominal, although:

The actual flight took place on May 8, 1983, but the day before, the initial count down had to be cancelled 5 minutes before blast-off, for meteorological reasons. The samples were then for the first time subjected to a full thermal process:

-melting,
-maintenance,
-controlled solidfication up to instant -120s,
-then natural solidification.

In regard to sample Al_3Ni-Al (furnace A), the TS4A instruction (cartridge base "cold") could not be complied with. Consequently, the cooling was slower and the thermal gradient was smaller than expected.

III - ANALYSIS OF THE THERMAL DATA

III.1. Data:

Telerecordings of four temperatures T_1, T_2, T_3, T_4 on the cartridges were made available by ERNO in numerical and graphic forms.

Numerical form:

This was expressed in the form of one point every second during the flight period only.

Graphic form (figures 2 and 3):

The first network of curves for a 75°C/cm, 2 mn/cm scale covers the entire thermal cycle: temperature rise, maintenance, cooling, until the rocket returns to the atmosphere. This allows the entire process to be properly controlled.

The second network of curves for a more expanded cycle (75°C/cm; 43 s/cm) covers the cooling period, i.e. the sample solidification periods prior to and during flight. Only these curves were analzyed extensively. The same type of curves for the reference samples was studied in the same way.

III.2. Method of analysis:

Each cooling curve was first read point by point, at the rate of one point every 50 seconds, using a digital-computer system.

From this we deduced: /8

III.2.1. A new form of cooling curves (figures 4 and 5) where the following were superimposed for each alloy:

- the temperatures read on the space cartridge,
- the temperatures read on the reference cartridge on the ground,
- the recommended temperatures.

III.2.2. A law of isotherm displacement on the cartridge surface in time.

At any instant t, the position $Z_T(t)$ of isotherm T may be directly deduced from the digitalized points using the interpolation formula:

$$Z_T(t) = Z_i + (Z_j - Z_i)\left(\frac{T - T_i}{T_j - T_i}\right)_t$$

where T_i and T_j are the values at instant t of the temperatures recorded at altitudes Z_i and Z_j selected in such a manner that

$$T_i < T < T_j .$$

While the thermocouples are evenly distributed along the cartridge, we still have

$$Z_j - Z_i = 33.3 \text{ mm (see figure 1).}$$

This law will serve to predict the solidification law of the sample.

III.3. • Variation of the isotherms on the cartridge surface: /9

From a point by point analysis of the thermal profiles at the cartidge leve, we see that any isotherm can be represented with good accuracy (~5%) using an empirical equation expressed in the following form:

$$\boxed{Z - Z_o = A_T(t - t_o)^{1,6}}$$

from which (assuming t_o and Z_o are the origins)

$$\boxed{\Delta Z_T = A_T \, \Delta t_T^{\,1,6}}$$

The exponent 1.6 is the same for all ground and space eutectic cartridges, relative to TEXUS IV and to TEXUS VI.

The factors A_T, t_o and Z_o are characteristic of temperature

T and may differ from one cartridge to another. They were optimized by iterative calculation applied to all isotherms of 50 in 50°C between 400 and 900°C.

For example, figure 6 shows the values of these factors in the case of an Al-Cu TEXUX VI cartridge, and figure 7 shows the isotherm network deduced from it. For a-posteriori reasons, we showed on this network the points directly obtained from the initial interpolation (3.2.2.).

The thermal profile on the cartridge surface is then known at each instant (figure 8).

To define the solidification conditions at the level of the growth interface, we decided to refer to the T_f melting isotherm of the eutectic, as in the case for the TEXUS IV experiment,

i.e. 548°C for Al_2Cu-Al,
and 640°C for Al_3Ni-Al.

Figures 9 and 10 show the curves representing the magnitudes deduced from this, namely:

- $\Delta Z = Z - Z_o$ — solidified length
- $V = \left(\frac{\partial Z}{\partial t}\right)_{T_f}$ — displacement rate of the solidification front
- $G = \left(\frac{\partial T}{\partial Z}\right)_t$ — thermal gradient at the interface level
- $\frac{G}{V}$ — ratio determining the interface stability and therefore the occurrence of a cellular superstructure.

These magnitudes were calculated at the cartridge level and could therefore not be considered definitive. Still, they give a very useful picture of the actual solidification conditions. Their numerical values at the characteristic flight instants are shown in table I.

	Characteristic Event	t (1) (s)	Δt	ΔZ mm	V $cm.h^{-1}$	G $K.cm^{-1}$	G/V $K.h.cm^{-2}$
T_f = 548°C Al_2Cu-Al sample	Onset of solidification	t_o = -460	0	0	0	54	∞
	Launch	0	460	4,5	5,6	47	8,4
	Microgravity onset	78	538	5,7	6,2	45,8	7,4
	End microgravity	437	897	13,0	8,4	40,4	4,8
	Return	570	1030	16,2	9,1	38,5	4,2
T_f = 640°C Al_3Bu-Al sample	Onset of solidification	t_o = -660	0	0	0	56	∞
	Launch	0	660	7,9	6,9	47,4	6,9
	Microgravity onset	78	738	9,5	7,4	46,2	6,2
	End microgravity	437	1097	17,8	9,4	40,7	4,3
	Return	570	1230	21,4	10,0	38,8	3,9

(1) Here, the instant of the rocket's launch was assumed to

be the time origin. It is interesting to note that if we wanted to reason in ΔZ and Δt, the isotherm displacement $T = T_f$ is represented to the nearest $\pm 1\%$ for all TEXUS IV and TEXUS VI eutectic cartidges (both space and ground), by the unique equation:

$$\Delta Z = 2.45 \cdot 10^{-4} \, \Delta t^{1.6}$$

(mm) (seconds)

III.4. Conclusion:

The ΔZ solidified lengths of the two samples, AlCu and AlNi, should therefore be respectively:

4.5 and 8 mm from the ground,
12 and 14 mm in flight, including
7 and 8 mm in microgravity

as we predicted (2.2).

The solidification rates have a relatively high mean value (7 to 8 $cm.h^{-1}$). The fact that these rates progressively increase during the experiment enables us to describe part of the λ-V diagram.

The ratio G/V drops fairly rapidly, which certainly leads to a rapid destabilization of the interface.

IV - SAMPLE ANALYSIS

IV.1. General observations:

The following was performed on the cartridges before they were opened:

-A visual examination.

-A sealing control using a helium spectrometer (by bleeding after immersion for 20 hours under 2 bars). No abnormality was found at this level.

-A gamma-radiograph (see figure 11) which shows that:

1. The volume-free compensating piston stayed exactly in the same place that it started in and therefore did not fulfill its function.

2. As for TEXUS IV, empty spaces were observed between the /13
cartridge base and the bottom of the crucible, and between the base of the crucible and the bottom of the cartridge. These two spaces, of about 0.5 mm each approximately, are not favorable for an optimum axial thermal transfer.

The following was performed on the samples after the cartridges were opened:

-A visual control.
-A photograph showing an overall picture under the two different angles (figure 12).
-A measurement of the surface roughness.
-A metallographic study.

No detrimental chemical interaction between the sample, cruicible and cartridge was found. No problems occurred when the charge was extracted. However, the boron nitride piston slides correctly upward, but not downward in those areas where the crucible walls were in contact with the liquid alloy.

As with the earlier experiments, the oxide surface layer covering the samples is striated with a network of fine cracks

coming from the differential dilation of the metallic sample and the oxide skin. One also observes a string of small bubbles 0.25 to 0.30 mm in diameter, and a large one of 2.5 mm in diameter. The surface roughness measurement did not show any large difference between the parts solidified under gravity and in microgravity.

IV.2. Metallographic observation: /14

The samples were observed on two scales:

-In a longitudinal section with small magnification (X2 to X10) to reveal the initial interface, the onset of the cellular superstructure and the interface markings coming from the sudden perturbation in the solidification process as the rocket is launched and upon its return in the atmosphere.

-In a transversal section with larger magnification (X300 to X1000) to characterize the eutectic periodic structure and its regularity.

IV.2.1 Sample preparation:

The samples were cut out longitudinally and transversally, according to the diagram below.

In the case of Al_2Cu-Al, the longitudinal section plane /15 should be perpendicular to the lamella: this direction is previously marked on the end of the monocrystalline seed.

The various surfaces are then mechanically polished using abrasive paper and diamond paste (up to 1 μm), then demonstrated chemically by immersion for 1 minute in the solution at ambient temperatures.

/1

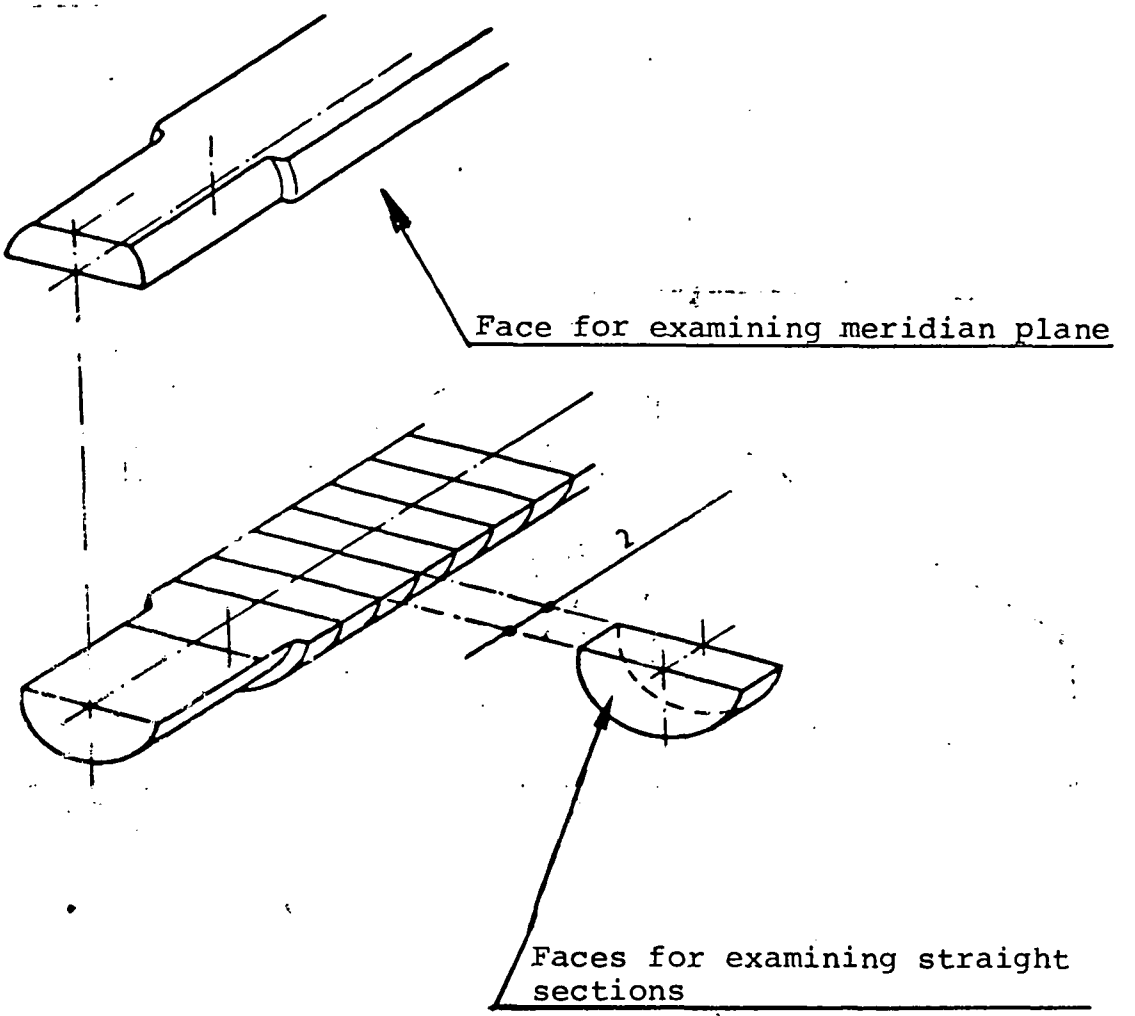

/1

HF	0.6%
HNO_3	3%
NCl	1.8%
H_2O	

IV.2.2. Macroscopic observation:

Figures 13 and 14 show an overall view of the space samples in a longitudinal section. We can easily see:

-the initial interface, which is duplicated in the case of the Al-Ni sample.

-a "clear" marking showing that the samples remelt as the

rocket returns to the atmosphere (opening of parachute).

-onset and variation of the lamellar structure.

In the case of the Al-Cu sample, another marking, this time diffused, is invisible in figure 13, but quite distinct in figure 15. This shows a slight perturbation as the rocket is launched.

Remark in regard to the initial interface:

Obviously, it alone appears in the ground samples. It is located at about the same height as in the Al-Cu samples (Z_o ground = 21 mm, Z_o flight = 24.3 mm, and this 3 mm difference agrees with the slight differences recorded in the thermal profiles).

Conversely, in the case of Al-NI, the initial interface of /16
the space sample is distinguishable not only by its morphology (dual marking), but also by its position ($Z_o$ground = 22.7 mm, $Z_o$flight = 14.6 and 15.3 mm). This cannot be explained by thermics, and reveals that the sample backmelts as the rocket is launched.

IV.2.3. Microscopic observations

-In longitudinal section:

Al-Al_2Cu: The metallographic observation makes it possible to characterize the curvature of the solidification front at the marking level. While the initial interface is flat, the backmelting interface corresponding to the atmospheric re-entry is convex (figure 15-a) and reveals cell boundaries. Figure 15-b represents the perturbed area during the launching which seems to show that the rocket is "spinning". Finally, at the initial interface (figure 15-c), one should notice the good epitaxy of the lamella on the seed which, contrary to the TEXUS IV

experiment, is performed without primary phase deposit.

Al-Al_3Ni: The initial interface is slightly convex, while the remelting interface is more flat. Small primary Al_3Ni dendrites have appeared (figure 16). The fibrous structure quickly turned into the heat flux, despite the absence of the initial seed.

-In transversal section:

The structures were analyzed by optical metallography and by diffraction of a laser beam.

Structural analysis by optical metallography: Figures 17 and 18 represent lamellar and fibrous structures selected among the various negatives taken, and considered to be the most regular. No improvement is seen in the regularity of the lamellar or fibrous structures between 1 g and 10^{-4}g. However, the sample part solidified in microgravity destabilized very rapidly, either because the interface had reached the critical destabilization rate, or because the drop in the gravity level promoted this destabilization. Unfortunately we do not have any sample lengths solidified in stable condition under microgravity which are large enough to judge the impact of microgravity on the regularity of the eutectic structures.

Structural analysis by laser diffraction: We showed that directional eutectic structures could be considered as light diffraction networks and that the analysis of diffraction images permits an evaluation:

-of the degree of perfection of the structure,
-of its direction,
-of its cycle. [6]

Figure 19 shows a few diffraction negatives of cross-sections of the Al_3Ni-Al TEXUS VI space sample with fibrous structure. The images here are approximately circles whose mean diameter makes it possible to establish the mean interfiber distance λ. Spots are sometimes seen which show a certain degree of organization in the fiber network.

Figure 20 shows the negatives of cross-sections of the Al_2Cu-Al space sample with lamellar structure. Besides the measurement of λ and an estimate of the structural regularity, these negatives show that the lamellar planes do not rotate in the growth phase.

Figure 21 shows a succession of diffraction negatives /18
of the longitudinal section of this same type of Al_2Cu-Al sample. As mentioned earlier, this section is perpendicular to the lamellar plane.

The analysis by laser diffraction confirms in quantitative mode that the structures obtained during the microgravity period are not more regular than those solidifed at 1 g, but on the contrary are more perturbed. This is what is brought to light when the diffraction spots are compared with one another: those relative to the sections of the region solified in microgravity are slightly more extended. The analysis integrates here a surface of about 1/4 of a square millimeter.

From all of these negatives, we may deduce the variation of the lamellar cycle as a function of the solidified length: λ (ΔZ).

V - DISCUSSION

V.1. Correlation between the thermal analysis and the macroscopic metallurgical observations.

In concluding the thermal study of chapter III, we

assumed that for all TEXUS eutectic samples the growth could be represented by the relationship:

$$\Delta Z = 2.45.10^{-4}\ \Delta t^{1.6} \qquad \begin{matrix}\Delta t \text{ in s} \\ \Delta z \text{ in mm}\end{matrix}$$

where $\Delta Z = Z - Z_o$ is the solidified length from the initial interface Z_o.

$\Delta t = t - t_o$ is the solidification time, counted from instant t_o when it actually begins.

Z is the interface position at instant t.

Furthermore, a macroscopic examination of the space samples revealed markings which we ascribed to specific events (figures 13, 14, 15, 16 - Chapter IV). /19

We are now going to show the coincidence between these two approaches, and specify instant t_o of the actual beginning of the solidification process. We will then proceed with an evaluation of the constitutional supermelting at the time of interfacial destabilization.

V.1.1. Case of the eutectic Al_2Cu-Al:

Comparison between the results of the thermal analysis and the marking positions:

Table II regroups 3 types of results, with respect to characteristic flight events:

1. The interfacial positions calculated from the displacement equation of the isotherm T_f = 548°C on the cartridge, i.e.

$$Z = 24.3 + 2.45 \cdot 10^{-4}\ (t + 460)^{1.6}.$$

2. The marking positions, ascribed to the various events, which prove to agree fairly well with the calculated values.

3. The interfacial positions, recalculated after determining the actual instant (t_o = -540 s) at which the solidification process begins, so as to match the slight marking observed at height Z = 30.1 mm, with the launching instant. The sample growth is then given by the formula:

$$Z = 24.3 + 2.45 \cdot 10^{-4} \, (t + 540)^{1.6}$$

The 0.6 mm deviation between the cumulated height for instant t_o = 570 s and the marking position therefore corresponds to the backmelting length. This result is probable; unfortunately it cannot be checked.

Table II

/20

Characteristic Event	t (s)	Interfacial position Z (mm)		
		calculated via isotherm equation (t_o = -460)	observed (markings)	recalculated with t_o = -540
Onset of solidification	t_o	24,3	24,3	24,3
Launch	0	28,8	30,1	30,1
Beginning of microgravity	78	30,1		31,5
End of microgravity	437	37,4		39,2
Return (parachute opening)	570	40,6	42	42,6

The growth diagram of the sample thus determined is shown in figure 26.

Evaluation of the constitutional supermelting at the time of destabilization:

In figure 13, we see the cellular structure at height Z = 32 mm (ΔZ = 7.7 mm), i.e. virtually right from the beginning of microgravity (Z = 31.5 mm). Referring again to the results of the thermal analysis on the cartridge wall, as shown in figure 9, we find that the following correspond to ΔZ = 7.7 mm:

-the soldification rate, $V=6.9\ cm\cdot h^{-1} = 1.92\cdot 10^{-3} cm\cdot s^{-1}$
-the temperature gradient $G = 44.2\ K\cdot cm^{-1}$.

From this, if we assume that the impurity responsible for destablization is characterized by a diffusion coefficient of about $D=5.10^{-5} cm^2 s^{-1}$, the constitutional supermelting value, according to Chalmers, is expressed:

$$\Delta T = D\frac{G}{V} = 1.15\ K.$$

V.1.2. Case of the eutectic Al_3Ni-Al /21

Comparison between the results of the thermal analysis and the marking positions:

Despite the difficulty caused by the backmelting of the sample when the rocket is launched, we tried to regroup the following results in table LII, while taking into account the characteristic flight events:

-The interfacial positions in the absence of backmelting, calculated from the displacement equation of the isotherm T_f = 640°C:

$$Z = 22.7 + 2.45.10^{-4} (t + 660)^{1.6}.$$

The initial length Z_o = 22.7 mm is in this case virtual: it is that of the reference sample seed on solified ground in rigorously identical thermal conditions (figure 5).

-The marking positions:

-initial virtual marking,
-backmelting interface to which no specific instant could be ascribed,
-return-marking, alone capable of offering a resetting capability.

-The interfacial positions, in the absence of backmelting, recalculated from the equation:

$$Z = 22.7 + 2.45.10^{-4} (t + 570)^{1.6}$$

in which the actual instant t_o = -570 s of the beginning of the resolidification process was evaluated using the following double assumption:

1. When the rocket returned, the solidification front had regained its position determined by the cartridge thermics (which seems to confirm the laser diffraction measurements, section V.2.2.).

2. The backmelting length on the rocket's return is 0.6 mm approximately, as for aluminum-copper.

The growth diagram is shown for the sample in figure 26.

Characteristic Event	t (s)	Interfacial position Z (mm)		
		Calculated via isotherm equation (t_o = -660)	observed (markings)	Calculated with t_o = -570
Onset of solidification	t_o	22,7	(22,7)	22,7
Launch	0	30,6		29
Beginning of microgravity	78	32,2	~1.5	30,4
End of microgravity	437	40,6		38,3
Return (parachute opening)	570	44,2	41,25	41,8

Table III

Evaluation of the constitutional supermelting at the time of destabilization:

The cellular structure appears at height Z = 29 mm, ΔZ = 6.3 mm.

Referring again to the results of the thermal analysis on the cartridge, we may deduce:

-the solidification rate $V=6.3\ cm\cdot h^{-1} = 1.75\cdot10^{-3} cm\cdot s^{-1}$,
-the temperature gradient $G = 48.7\ K\cdot cm^{-1}$,

i.e. a constitutional supermelting value of:

$$\Delta T = D\frac{G}{V} = 1.4K.$$

However, the launch certainly caused: /2

-the liquid phase to mix resulting in a drop in the temperature gradient,

-the need for the backmelting to be followed by accelerated resolidification, in order to establish coincidence with the thermal field on the cartridge.

The G/V ratio at the solidification front was overvalued for two reasons. Conversely, the mixing effect also decreases the size of the interfacial diffusion layer, which generally stabilizes the interface [8]. These antagonistic effects lead us to consider that the order of magnitude of the calculated supermelting is simply indicative.

V.2. Correlation between thermal analysis and microscopic metallurgical observations: Study of the relationship λ-V:

In chapter IV, we reported the results of the qualitative microscopic observations of the samples. Here, we will try to come to some quantitative conclusions on the laser diffraction negatives.

As of now, we actually have two types of information, namely:

1. Direct measurement of the λ cycle of the eutectic structures, all along the samples.

2. The crystal growth law deduced from the thermal analysis:

$$Z = 2.45.10^{-4} \ \Delta t^{-1.6} \qquad \left| \begin{array}{l} \Delta z \text{ in mm} \\ \Delta t \text{ in s} \end{array} \right.$$

from which we may deduce a law relative to the growth rates:

$$V = 8.86.10^{-3} \ \Delta Z^{0.375} \qquad \left| \begin{array}{l} V \text{ in mm.s}^{-1} \\ \Delta z \text{ in mm} \end{array} \right.$$

or

$$V = 3.19 \ \Delta Z^{0.375} \qquad \left| \begin{array}{l} V \text{ in cm.h}^{-1} \\ \Delta Z \text{ in mm .} \end{array} \right.$$

V.2.1. Case of the alloy Al_2Cu-Al /24

In reporting the logarithmic coordinates, the Δ measurements, functions of the solidified distance ΔZ (figure 22), it seems that most points fall on the straight line of the equation:

$$\lambda = (3.5 \pm 0.2)\ \Delta Z^{-0.187}.$$

The farthest points from the straight line are respectively:

-those located right next to the initial interface, which is easily explained by the uncertainly concerning the Z location of the sections which, after sectioning and polishing, may be estimated to be $|\delta Z| = 0.2$ mm, which leads to a relative error

$\frac{\delta(\Delta Z)}{\Delta Z} = 200\%$ when $\Delta Z = 0{,}1$ mm

40% when $\Delta Z = 0{,}5$ mm

20% when $\Delta Z = 1$ mm

10% when $\Delta Z = 2$ mm

-those found in the "perturbed" region of the first marking ($Z = 30.1$; $\Delta Z = 5.8$).

-those relative to a high value of ΔZ ($\Delta Z \gtrsim 16$ mm) for which the cellular superstructure is very marked and as a result the relative error on λ is high.

The log λ - log V curve (figure 23) has the same appearance and calls for the same remarks: most experimental points fall on a straight line of the equation:

$$\lambda^2 V = 39 \pm 10\% \qquad \left| \begin{array}{l} \lambda \text{ in } \mu m \\ V \text{ in } cm.h^{-1} \end{array} \right.$$

Several conclusions may be drawn on examining curves 22 and 23: /25

First, the agreement is remarkable between the direct measurements of λ via laser diffraction, the analysis of the thermal readings and the law $\lambda^2 V$ = Cste.

The 23% deviation between the value thus determined of the constant, and its value announced in chapter I, does not seem to be very significant. A systematic error of 11% on the measurements of λ, which is plausible, would suffice to explain this.

Now that the validity of the growth law Z(t) is well established, it is possible to demonstrate in figures 22 and 23 the interfacial positions at the characteristics instants and the corresponding growth rates: we then observe that the law $\lambda^2 V$ = Cste is not affected by the gravity level, as the value of the constant remains the same at 1g and in microgravity.

V.2.2. Case of the alloy Al_3Ni-Al

The conclusion on the Al_2Cu-Al sample lead us to assume:

-that the growth law, in the absence of backmelting, is indeed that deduced from the thermal analysis

$$\Delta Z = Z - 22.7 = 2.45.10^{-4} \ (t + 570)^{1.6}$$

-that a large backmelting occurred in the Al_3Ni-Al sample when the rocket was launched and a small backmelting on its return.

These assumptions are confirmed by the cycle measurements via laser diffraction and this gives us a numerical value for the constant:

$$\lambda^2 V = \text{Cste} = 35.$$

This value concerns only the sample portion solidifed in microgravity. We have no information about the part solidified in λg, which disappeared after backmelting.

We shall now present the λ-Z diagrams (figure 24) and V-Z (figure 25) upon which we have shown: /26

a. The experimental points (average of the λ measurements in the various sections),

b. The expected λ-Z and λ-V curves in the absence of backmetling (the λ-V conversion being obtained from $\lambda^2 V = 35$).

The characteristic points are shown on these curves: launch, beginning and end of microgravity, return. We then observe that the curves are made up of 3 segments:

-A central segment (a) ($33 \leq Z \leq 41.25$) including the 8 mm of sample preceding the "return" marking. The constant $\lambda^2 V = 35$ was adjusted so that this segment coincides with the predetermined curve, and the perturbation effect due to the launching seems to be forgotten at the end of the flight.

-An initial segment (b) relative to the sample growth, from the backmelting interface (initial marking Z = 14.6/15.3 mm) in conditions of thermal imbalance between the actual interface position and its expected position in the absence of backmelting.

As the system tends to regain its equilibrium, it is normal to observe a higher rate of interfacial progression, and therefore a smaller λ cycle.

-The plotting of the final segment (c), following the return-marking, is purely indicative: only one experimental point appears here, but its characteristics (low λ - high V) express a deviation following a perturbation.

Conclusions conerning Al_3Ni-Al

The only experimental points for which we may try to check the law $\lambda^2 V$ = Cste corresponding to solidification in microgravity. The value of the constant is distinctly higher (+40%) than announed in chapter I, which does not explain the only measuring error on λ, evaluated to be $\pm$ 10%.

The backmelting due to the rocket launch not only suppresses the entire part of the sample solidified on the ground prior to the launch, but perturbs the solidification conditions at the beginning ofthe flight: any objective comparison of the structures obtained at 1-g and in microgravity has become impossible.

The values of the interfiber cycle found in microgravity therefore seem to be systematically higher than those deduced from the law obtained under normal gravity. This conclusion, as we have seen, should be considered with much precaution. In in no case does it confirm the drop in the microgravity cycle observed by Pirich et al. in the Mn-Bi system during the SPAR rocket flights.

VI - CONCLUSION

The experiments performed on the Al-Cu and Al-Ni eutectics during the TEXUS IV and TEXUS VI flights proved, like the experiments on germanium doped in gallium in the same programs, the feasibility of solidifications directed in microgravity during the rocket's free fall. Perturbations associated with the launch and atmospheric return do not dramatically perturb the solidification course.

We have shown from the thermal analysis made on the outside thermocouples on the cartridge that it is possible to derive information about the growth conditions (solidification rate and thermal gradient), in agreement with the localization of marking events in the samples: initial front, backmelting at the time of atmospheric re-entry. However, it is clear that the thermal analysis would be more accurate if it were possible to have temperature readings of the samples themselves (i.e. within the cartridges).

It should be pointed out that the TEM 03 furnace is not /28 fully adapted to the targetted program:

-The thermal gradient in the cartridge is generally too low, which causes premature destabilization of the solidification front.

-The curvature of this front changes throughout the experiment.

-Finally, the gradient and velocity values are not stationary during the solidification process.

The main conclusions obtained on regular solidification from this experimental program are the following:

1. The optical observation and the analysis via laser diffraction of the microstructures, contrary to Hasenmeyer's statements (Skylab program), did not show any improvement in the regularity of the lamellar or fibrous structures, but rather a deterioration in these, which are certainly linked to the rapid destabilization of the solidification front during the microgravity cycle. The conclusions of these experiments are therefore only partial and the Spacelab FLSP mission should give us more meaningful answers about the impact of gravity on the perfection of eutectic structures.

2. The constitutional supermelting at the destabilization threshold was evaluated for the Al-Cu sample and the Al-Ni sample at $\Delta T^* = 1.15$ and 1.4 K respectively. This supermelting is undoubtedly associated with eh presence of noncontrolled impurities in the liquid baths, ontroduced when the charges were being prepared.

3. Finally, the λ-V relationship between structural periodcity and growth rate were studied in an unsteady steat in a fairly broad velocity spectrum $(2 \leq V \leq 11\ cm.h^{-1})$.

In the case of the lamellar eutectic Al-Al_2Cu, we may state /29 that the lamellar cycle is not affected by the gravity level.

For the fibrous eutectic Al_3Ni-Al, we were not able to be so affirmative. The TEXUS VI experiment established a 18% higher value for the microgravity cycle than for the corresponding values traditionally established on the ground.

Due to the backmelting, at the time of the rocket launch, over the entire length previously solidified on the ground, this experiment does not give any information on the value of the 1 g cycle. However, if a variation of the fibrous cycle exists in microgravity, it does not seem to confirm the large drop of 35% found on the Mn-Bi eutectic by Grumman's American team.

REFERENCES

1. Y. Malmejac, Thesis, Grenoble (1971).

2. F.D. Lemkey, R.W. Hertzberg and J.A. Ford, "The Microstructure, Crystallography and Mechanical Behaviour of Unidirectionally Solidified Al-Al_3Ni Eutectic", in: Transactions of the Metallurgical Society of AIME , Vol. 233, Feb. 1965, pp 334-341.

3. Ron G. Pirich and D.J. Larson, Jr. "SPAR VI Technical Report for Experiment 76-22. Directional Solidification of Magnetic Composites", in: Grumman Research Department Report RE 602 , July 1980.

4. Hasenmeyer, Skylab Mission, NASA Report 1973.

5. J. de Goer, J.J. Favier and R. le Maguet Solidification dirigee du systeme eutectique Al_2Cu-Al en fusee-sonde. Exploitation de l'experience TEXUS IV. Preparation de l'experience TEXUS V-VI (Directional Solidification of the Al_2Cu-Al eutectic system in a sounding rocket. Analysis of the TEXUS IV experiment. Preparation of the TEXUS VI-IV experiment"). DMG Report No. 41/82.

6. J.J. Favier, J.P. Morlevat and J. Duvernoy, "Method of Analysis of the Regularity of Lamellar Eutectic Structures by Diffraction of a Laser Beam", in: Metallurgical Transactions B. vol. 14-B, March 1983, pp 105-108.

7. J.J. Favier and A. Rouzaud, to appear in Journal of Crystal Growth

Cartridge for TEXUS VI experiment "directed solidification of doped semiconductors and eutectic alloys"

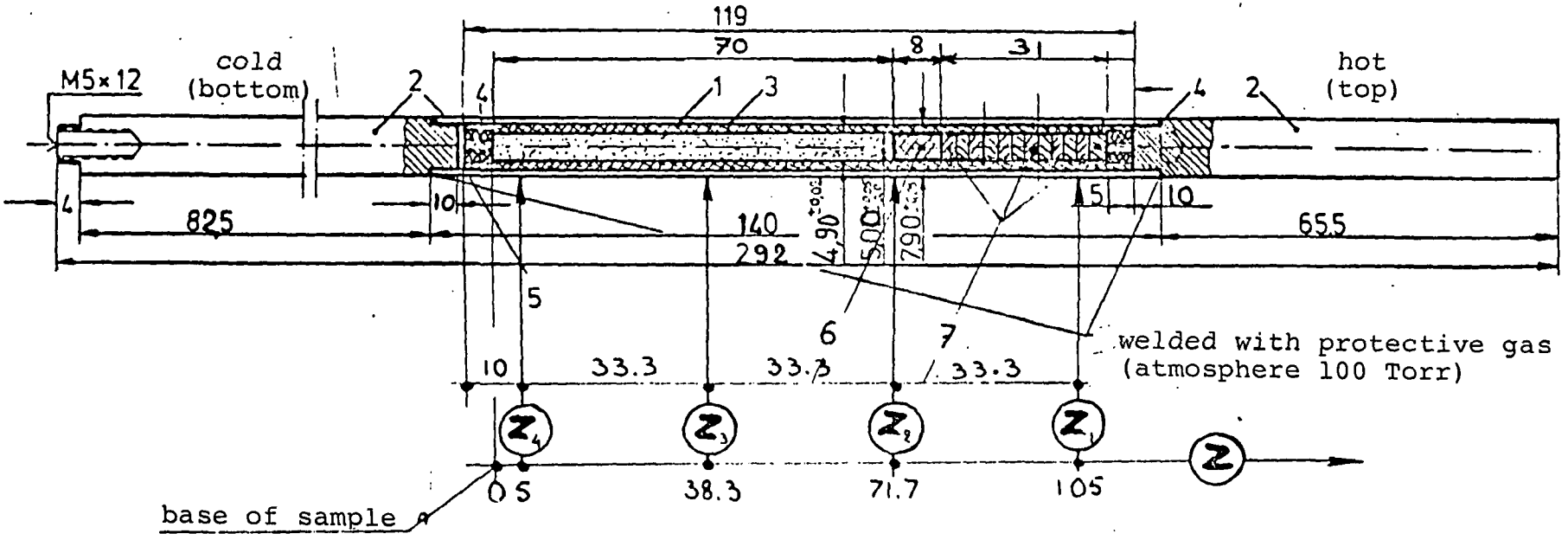

sample	Al-Al$_2$Cu // Al-Al$_3$Ni	1
cartridge	tantalum	2
crucible	Boronnitride	3
thread stopper	Boronnitride	4
fiber laver	Al_2O_3	5
piston	Boron nitride	6
Elastic felt	Graphite	7

Name			Material	Section
	Tag	Name		
gez.	18.3.81	G. Ahl	cartridge for TEXUS V experiment	
gepr.	18.3.81	de Goër		

Figure 1

-Cartridge-sample system

-Position of thermocouples

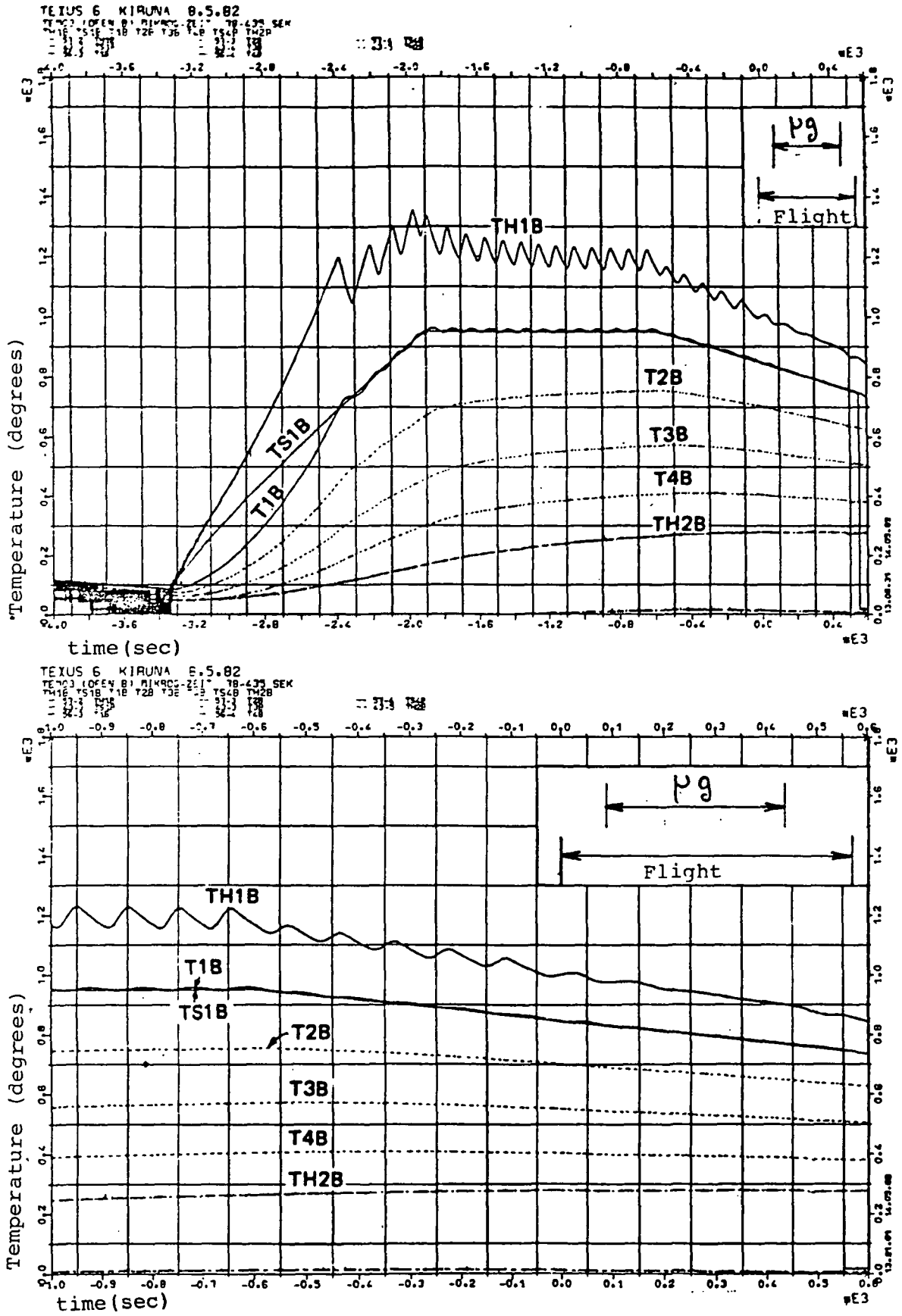

Figure 2. - Temperature reading in furnace B (Al_2Cu-Al).

T_1, T_2, T_3, T_4: Temperatures on cartridge wall
T_{S1} : Recommended temperature relative to T1
$T_{S4} = 0$: No recommendation relative to T4
T_{H1}, T_{H2} : Temperatures at the heating elements level.

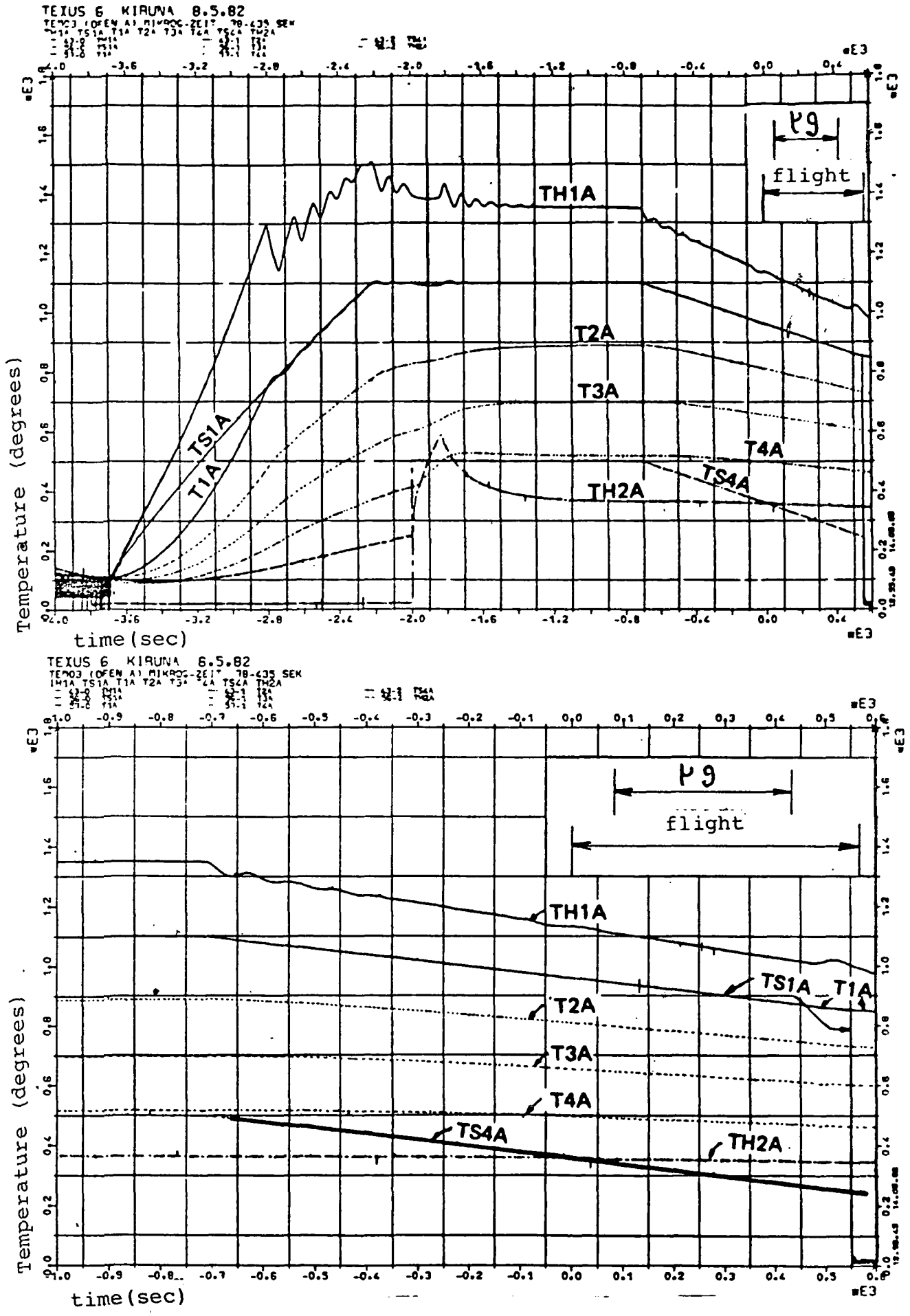

Figure 3. - Temperature readings in furnace A (Al_3Ni-Al).

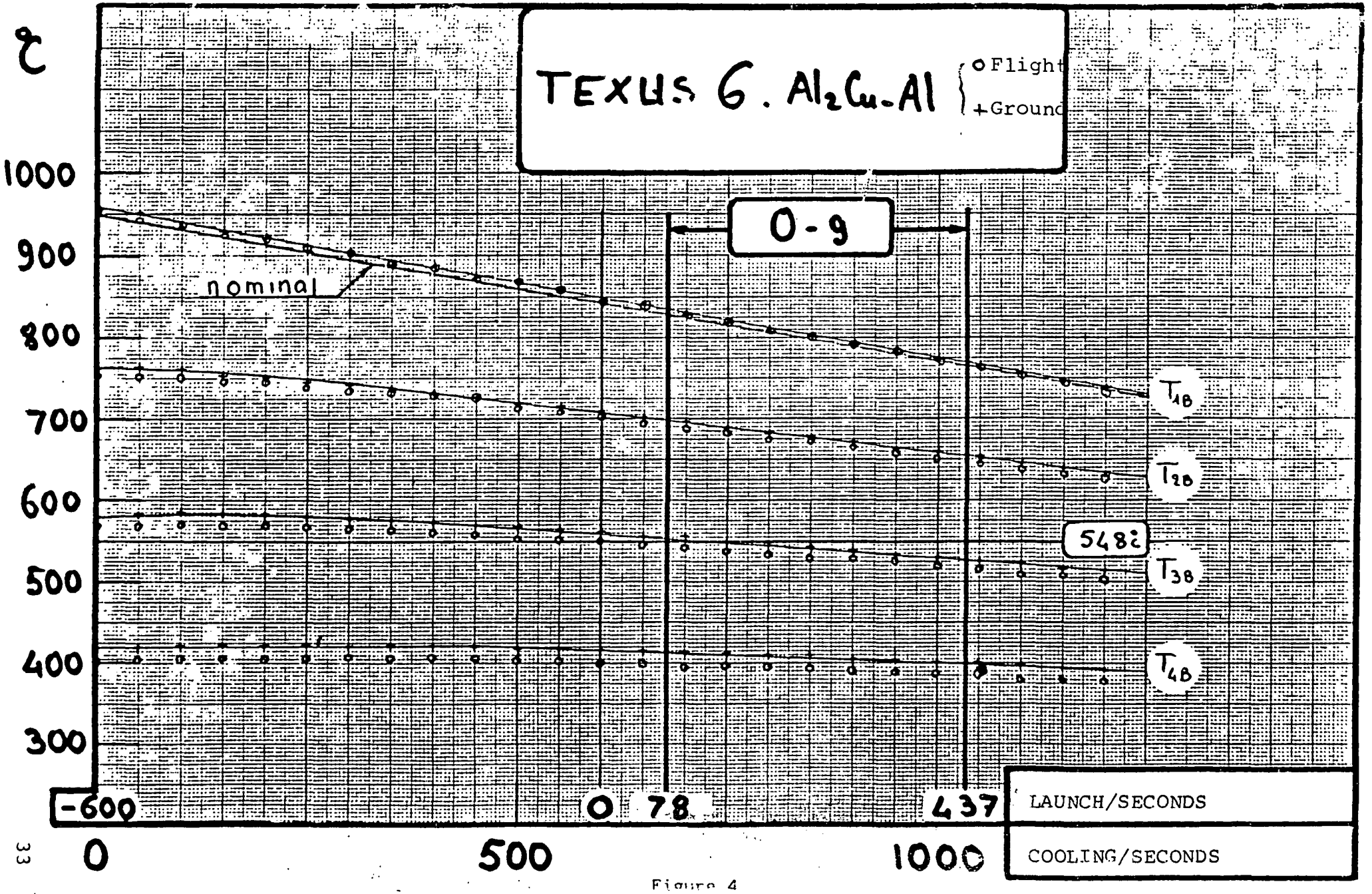
TEXUS 6. Al_2Cu-Al
o Flight
+ Ground
0-9
nominal
T_{1B}
T_{2B}
5482
T_{3B}
T_{4B}
T
1000
900
800
700
600
500
400
300
-600
0
78
437
0
500
1000
LAUNCH/SECONDS
COOLING/SECONDS

Figure 4

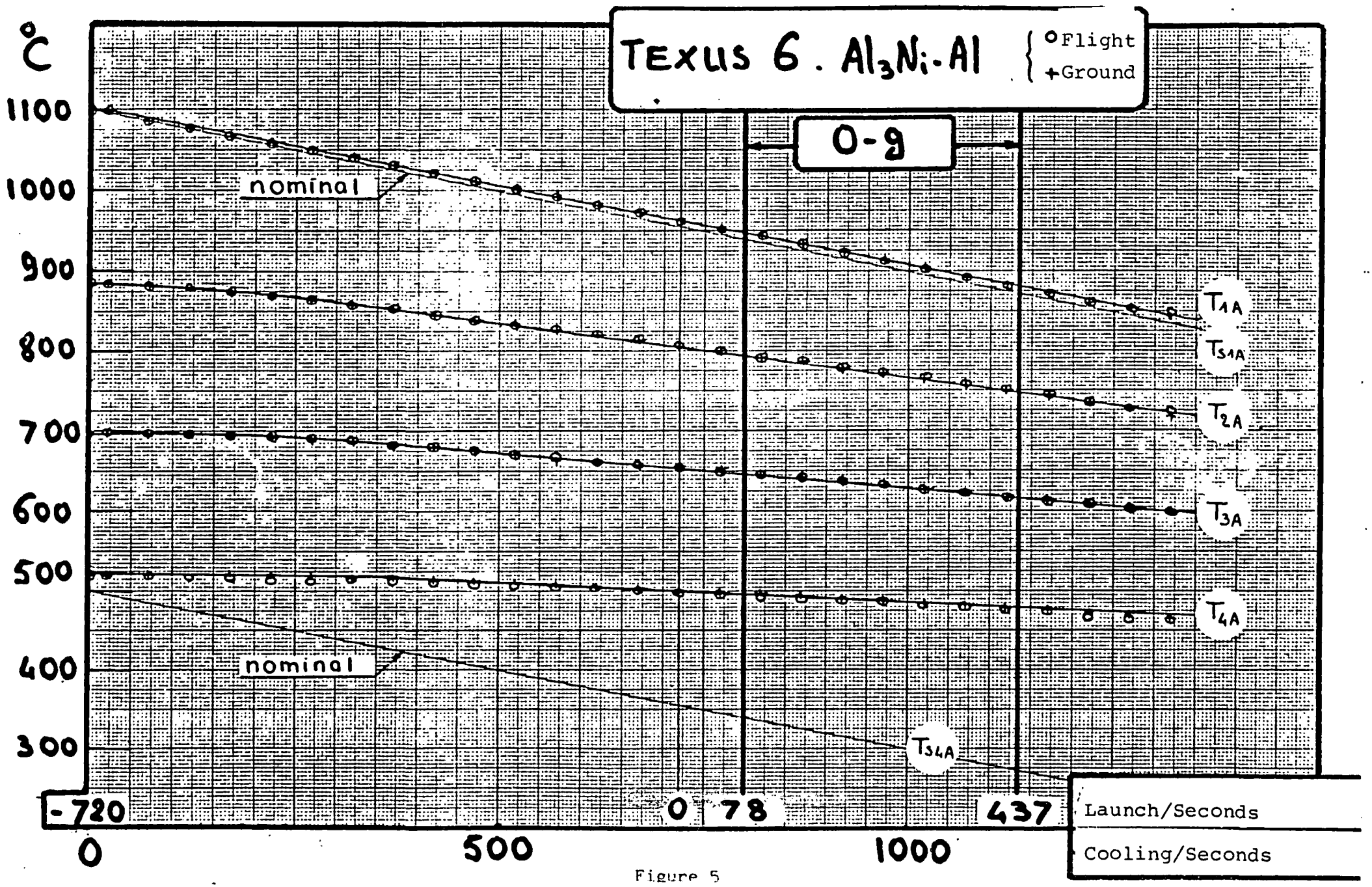
TEXUS 6 . Al_3Ni-Al
°Flight
+Ground
0-g
°C
1100
1000
900
800
700
600
500
400
300
nominal
nominal
T_{1A}
T_{S1A}
T_{2A}
T_{3A}
T_{4A}
T_{S4A}
-720
0
78
437
500
1000
Launch/Seconds
Cooling/Seconds

Figure 5

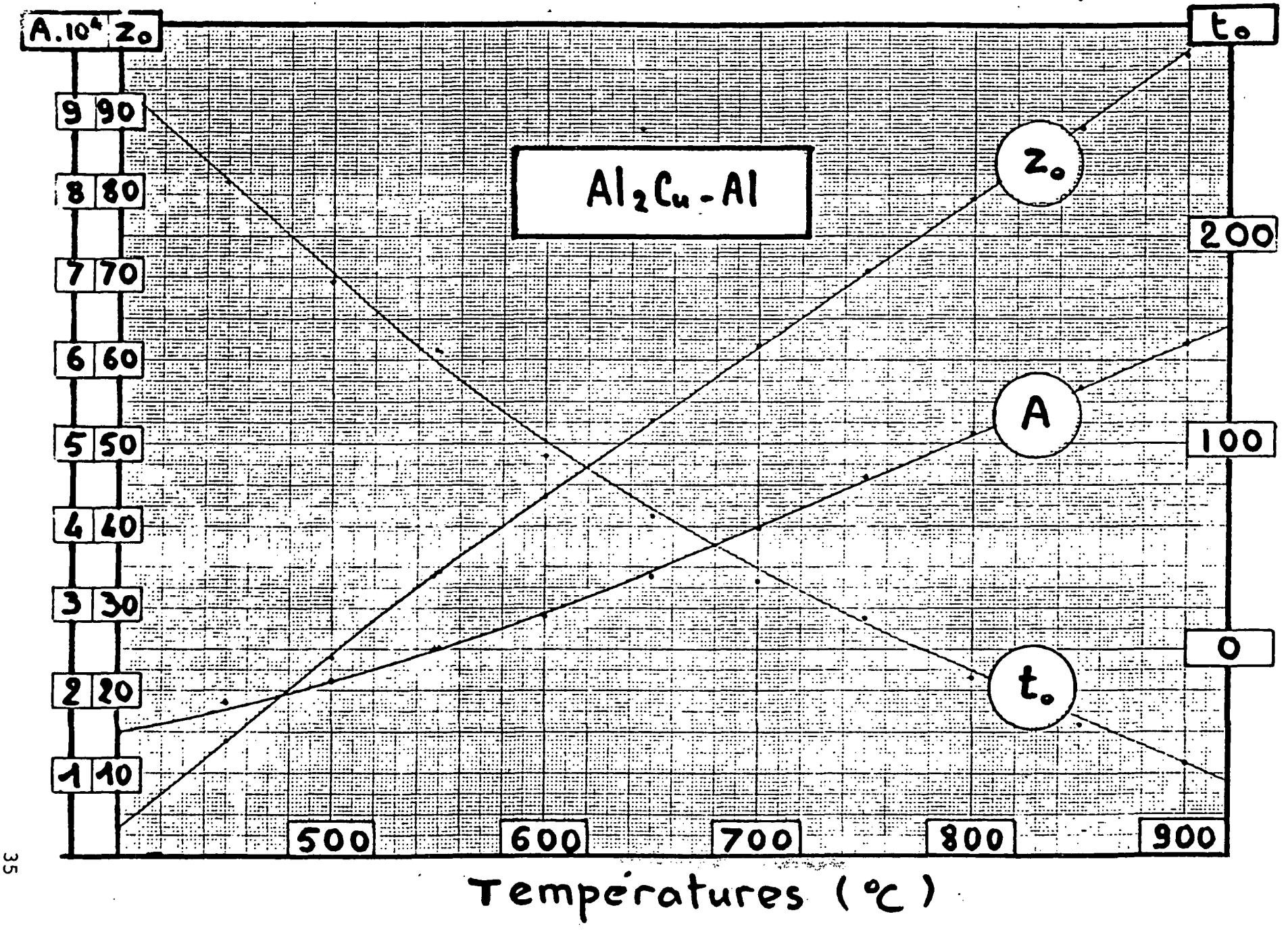
A.10⁴ Z₀
9 90
8 80
7 70
6 60
5 50
4 40
3 30
2 20
1 10
Al₂Cu - Al
Z₀
A
t₀
t₀
200
100
0
500
600
700
800
900
Températures (°C)

Figure 6

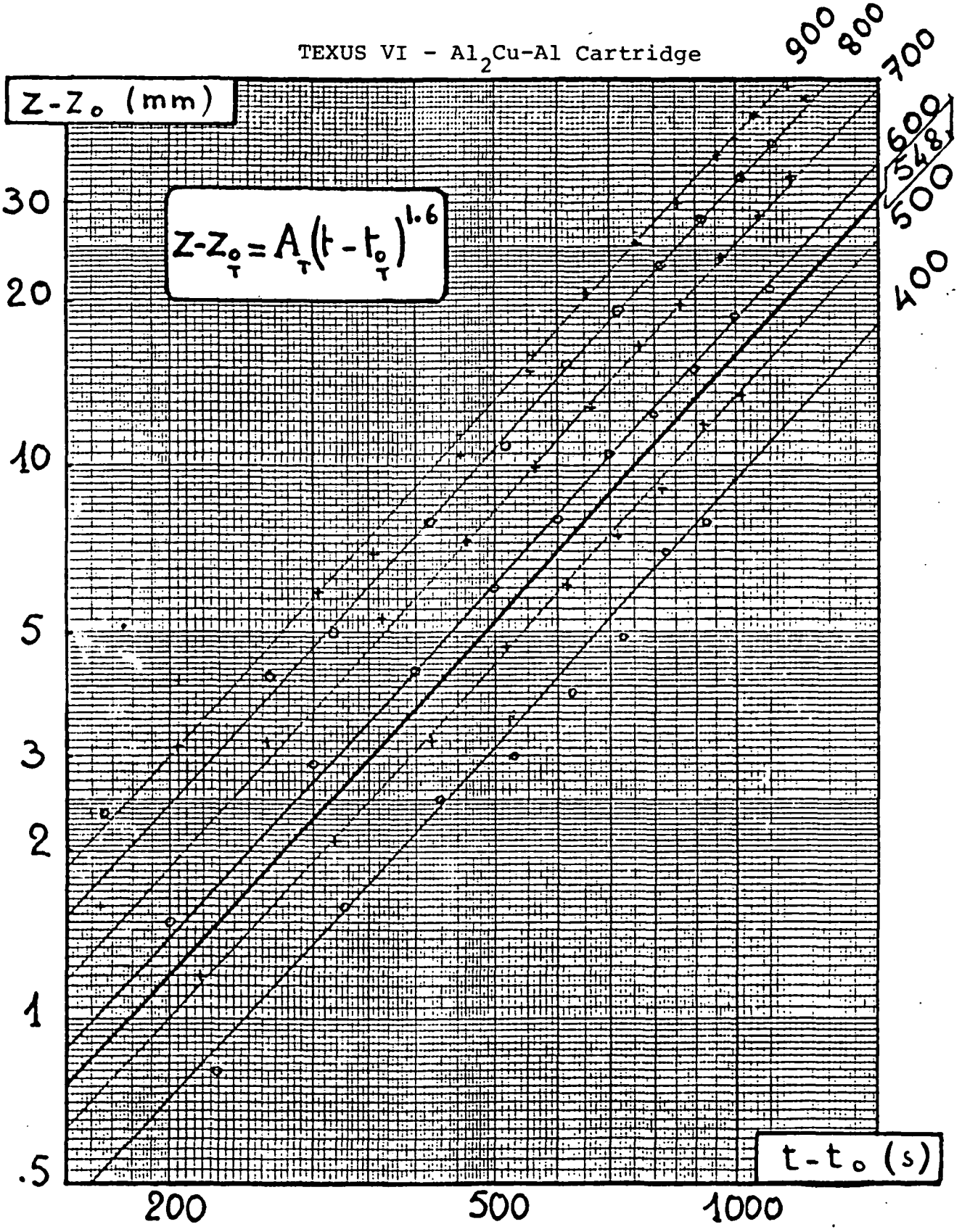

Figure 7

Isotherm Network

TEXUS VI - Al_2Cu-Al flight cartridge

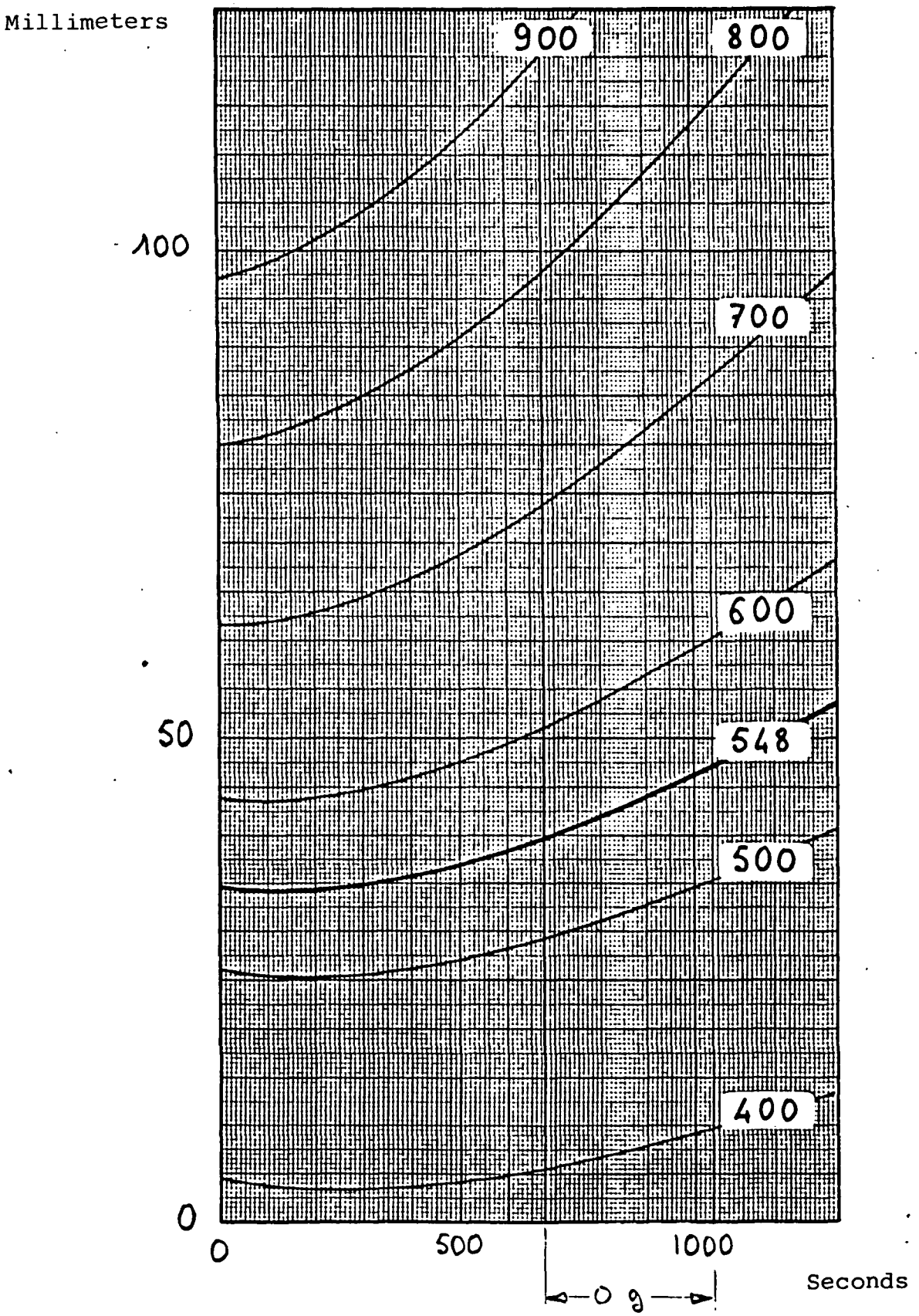

Figure 8
Isotherm Network

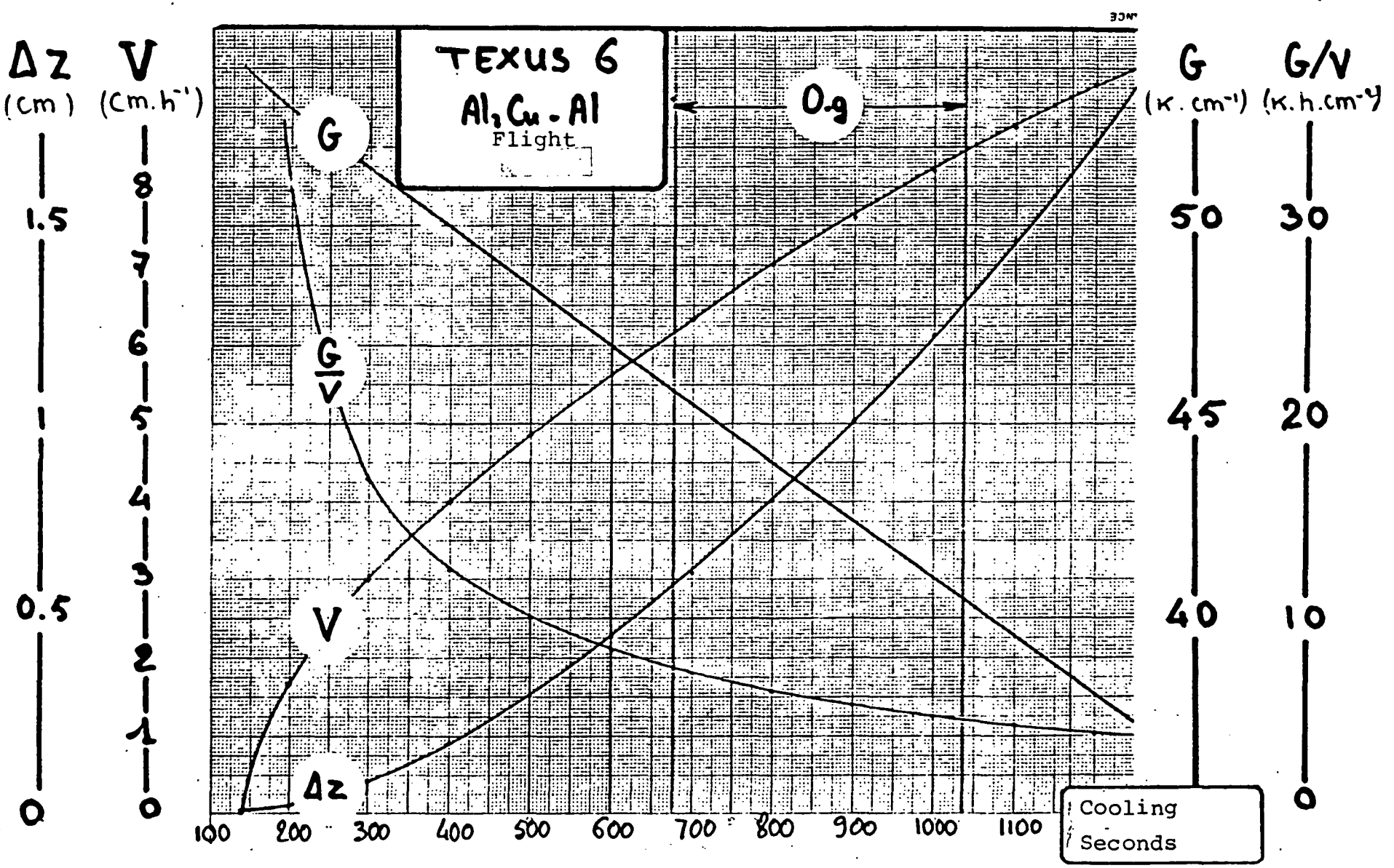
TEXUS 6
Al, Cu - Al
Flight
0.g
G
G/V
V
Δz
ΔZ (Cm)
V (Cm.h⁻¹)
G (K.cm⁻¹)
G/V (K.h.cm⁻²)
1.5
1
0.5
0
8
7
6
5
4
3
2
1
0
50
45
40
30
20
10
0
100
200
300
400
500
600
700
800
900
1000
1100
Cooling
Seconds

Figure 9

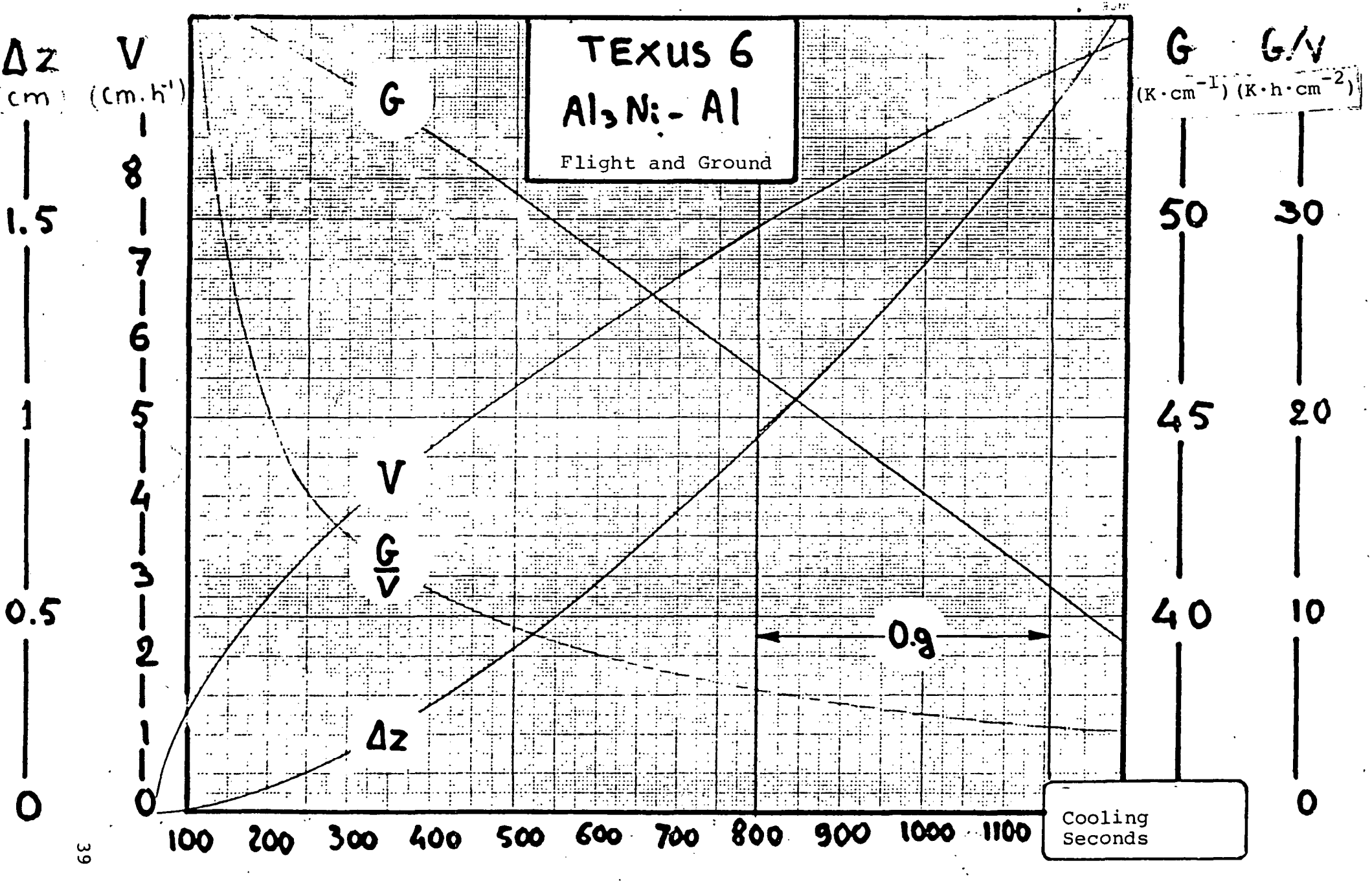
TEXUS 6
Al3Ni - Al
Flight and Ground
Δz
cm
V
(cm.h⁻¹)
G
(K·cm⁻¹)
G/V
(K·h·cm⁻²)
G
V
G/V
Δz
0.g
Cooling
Seconds
0
0.5
1
1.5
0
1
2
3
4
5
6
7
8
40
45
50
0
10
20
30
100
200
300
400
500
600
700
800
900
1000
1100

Figure 10

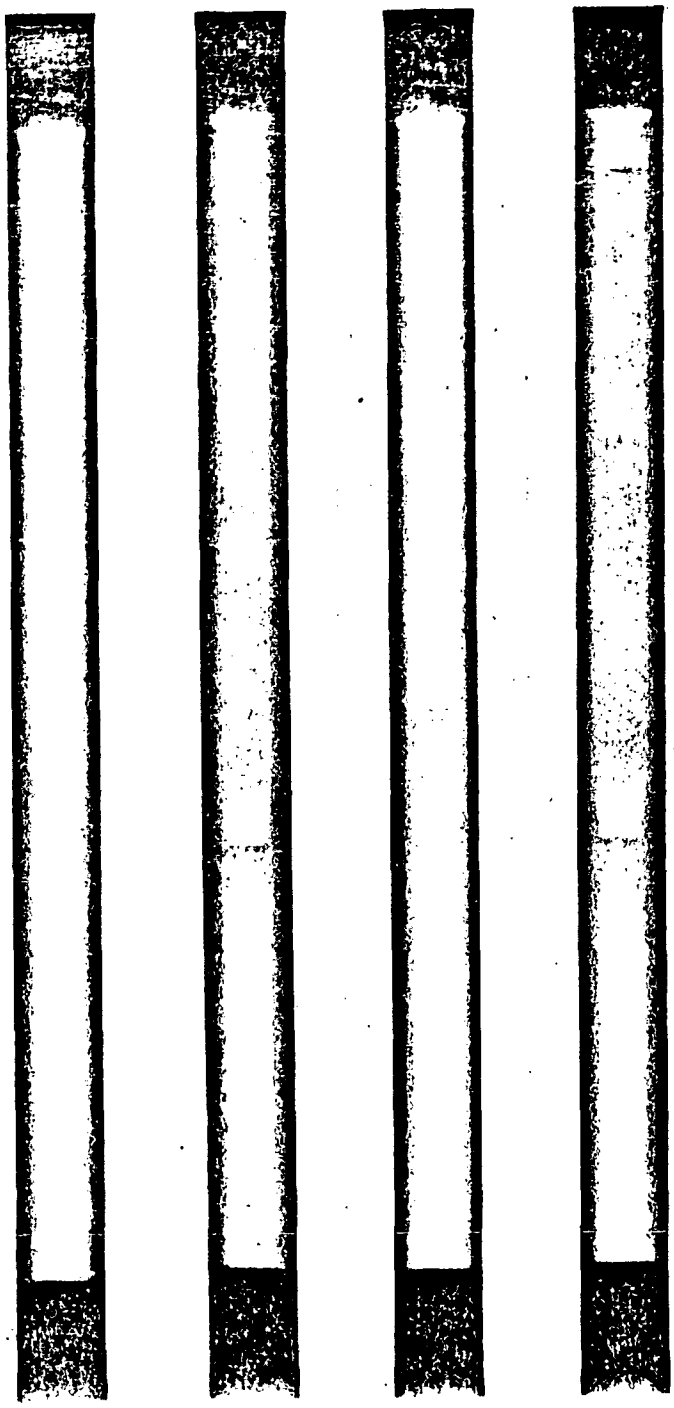

Figure 11

TEXUS VI - γ radiography of cartridges after flight.

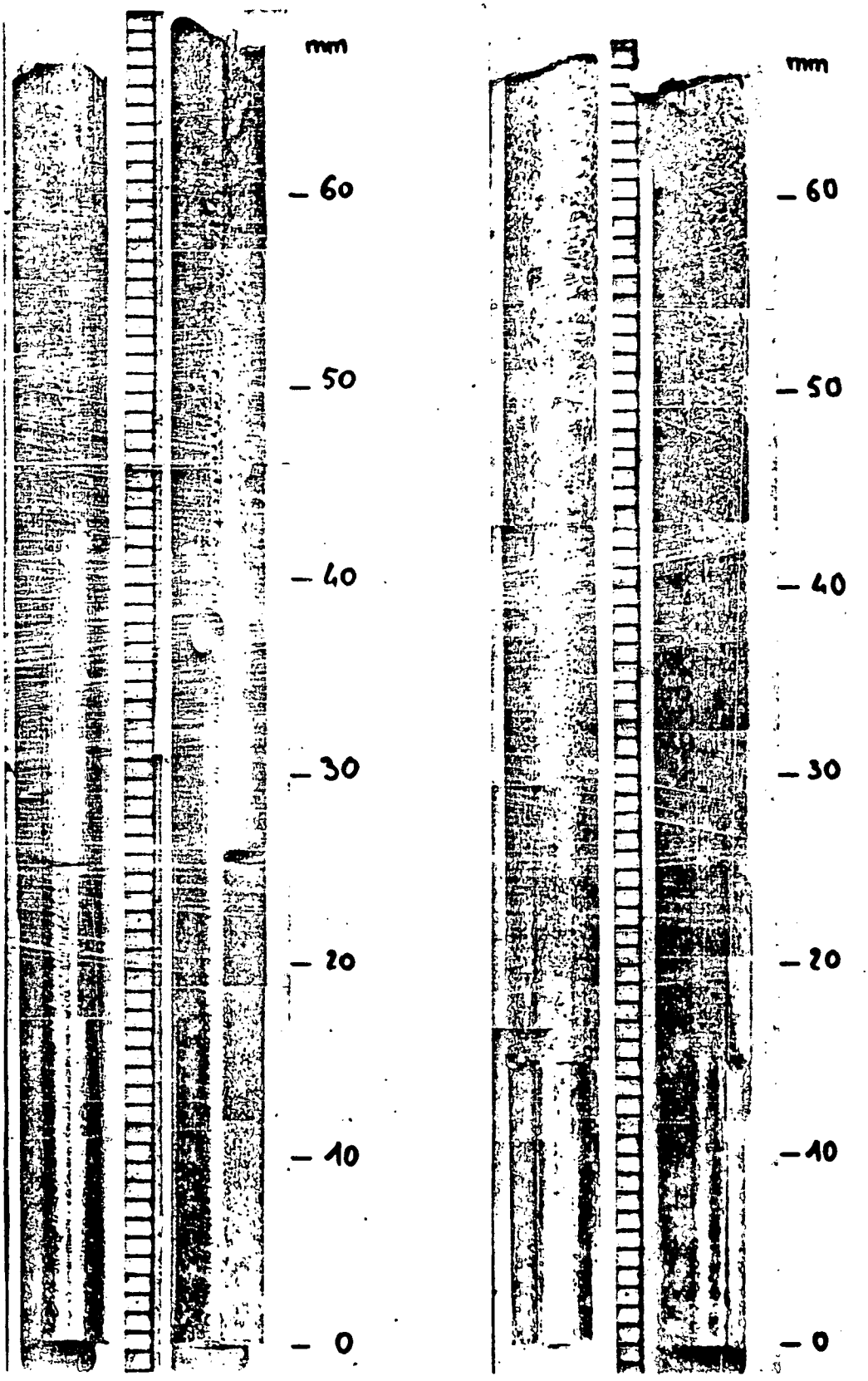

Figure 12

Photography of solidified samples during the TEXUS VI mission.

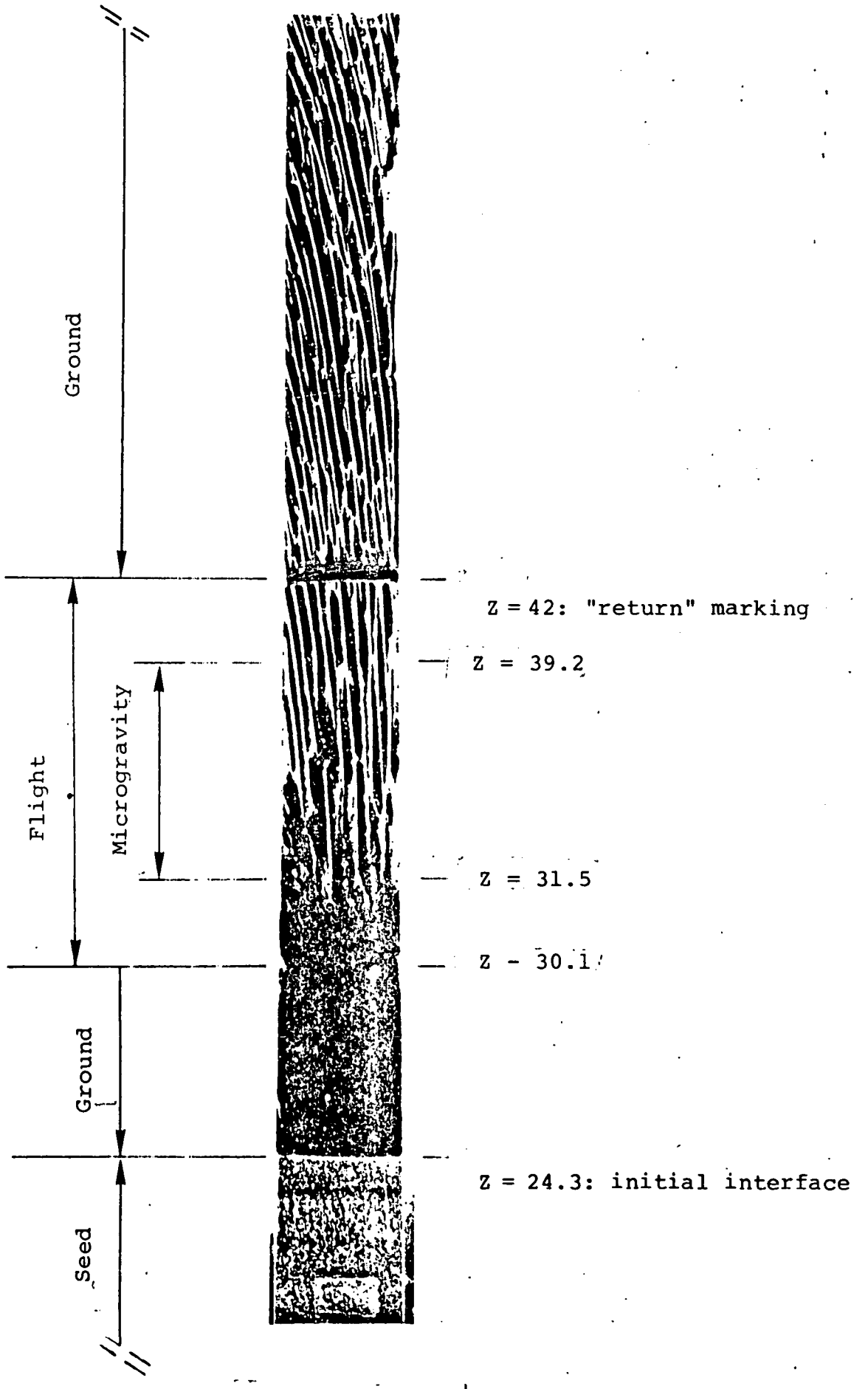

Figure 13
Longitudinal section of the Al_2Cu-Al sample

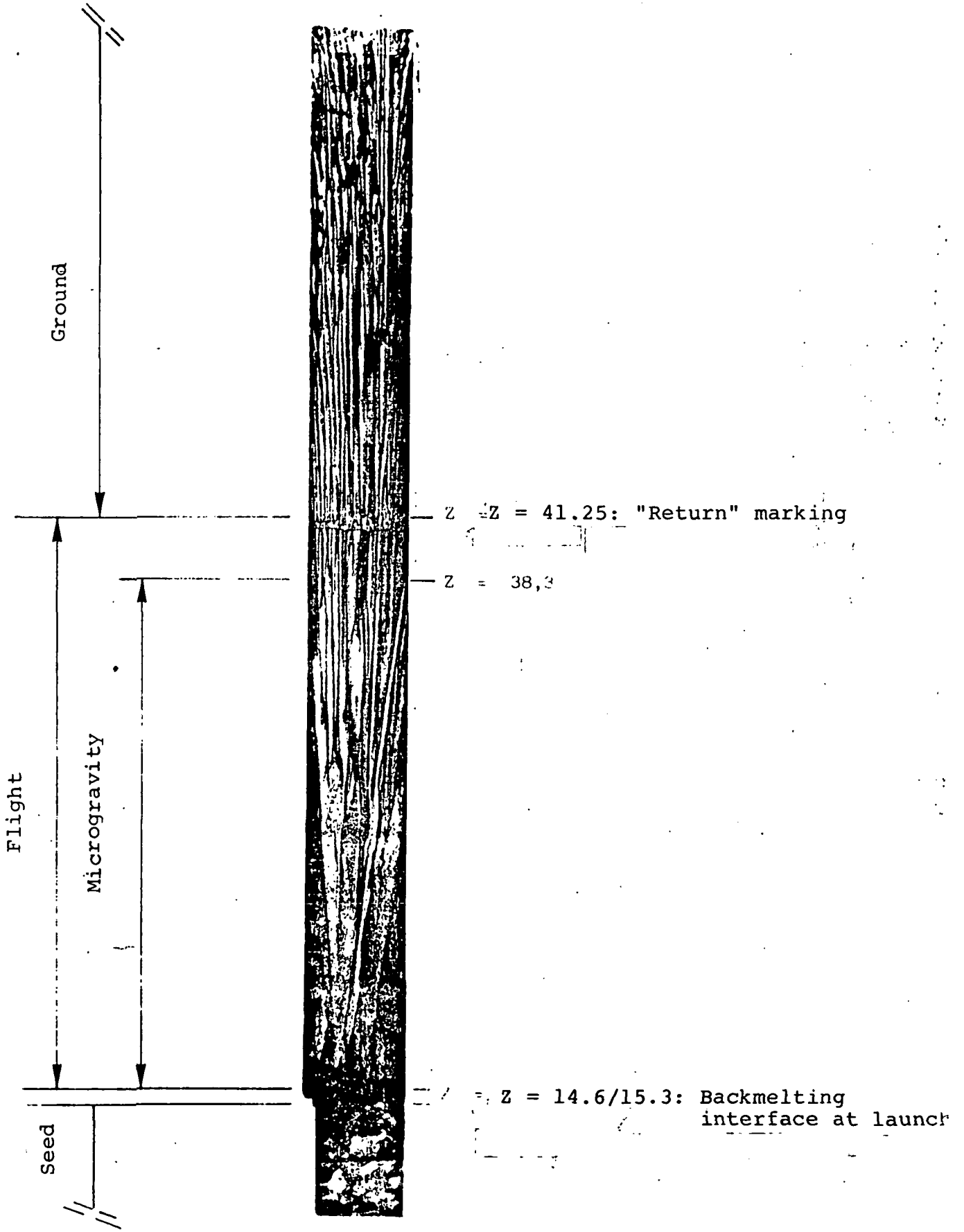

Figure 14
Longitudinal section of the Al_3Ni-Al sample

Al_2Cu-Al Sample - longitudinal structure

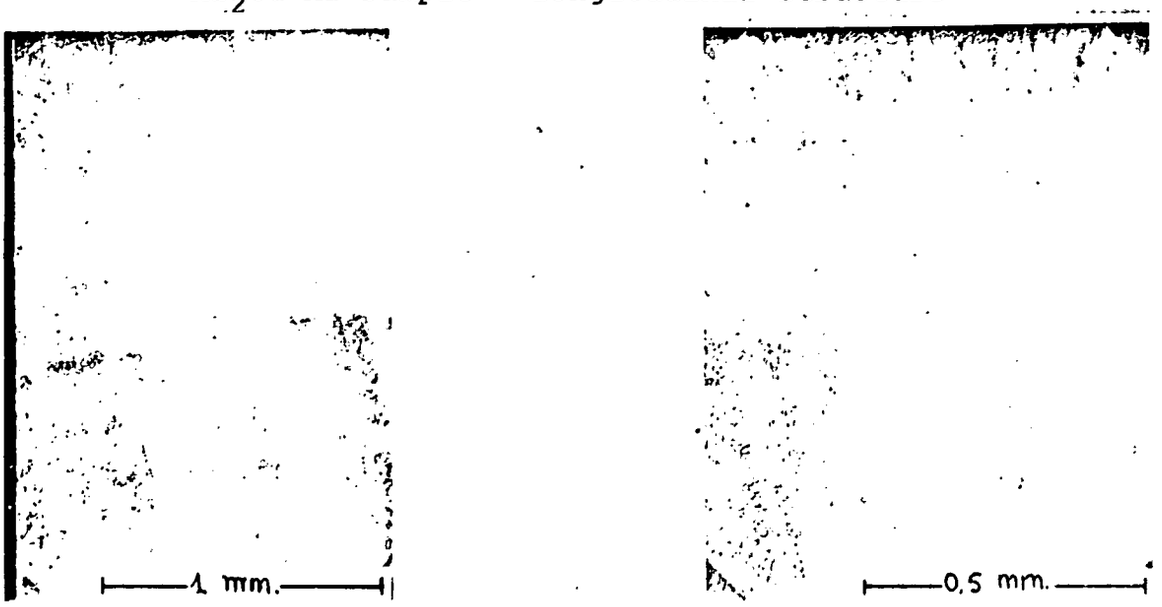

Figure 15-a

Backmelting interface on return (Z - 42 mm)

Figure 15-b

Perturbation at launch (Z - 30.1 mm)

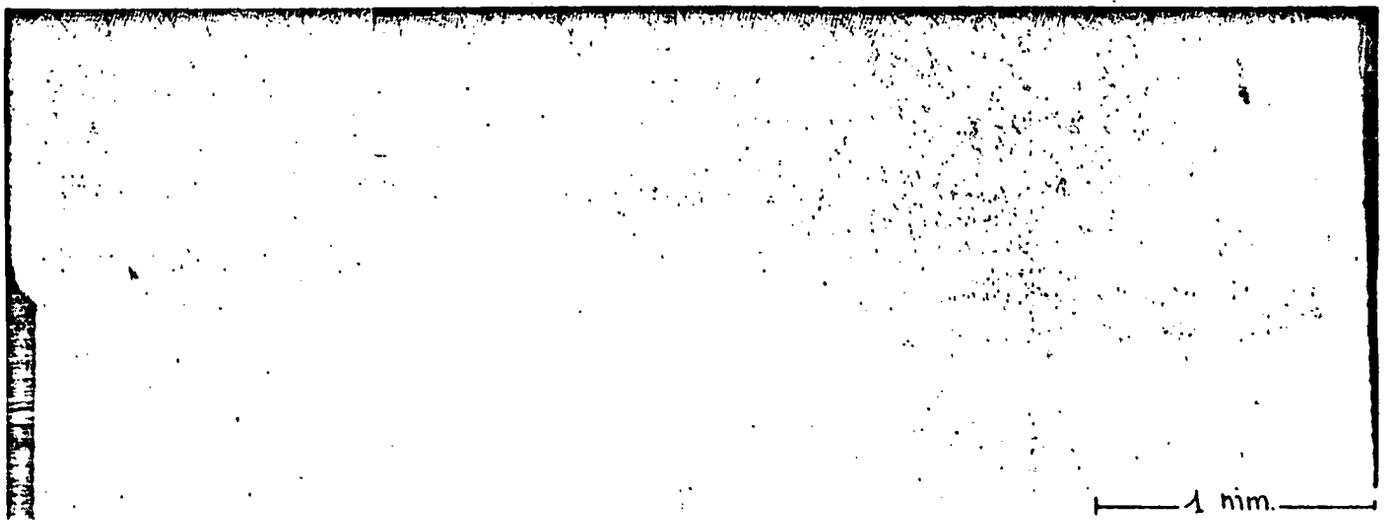

Figure 15-c

Initial interface (Z = 24.3 mm)

Al_3Ni-Al sample: longitudinal structure

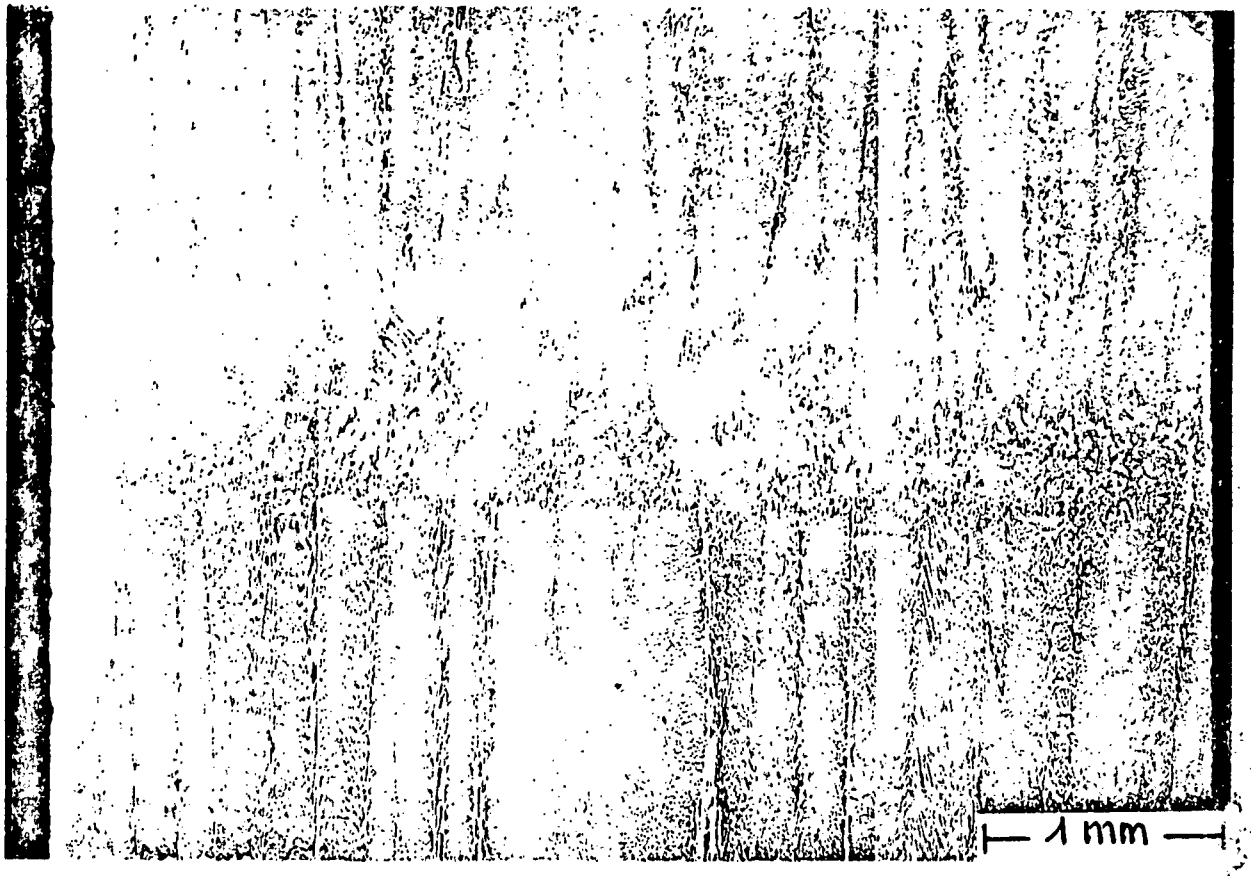

Figure 16-a

Backmelting interface on return (Z = 41.25)

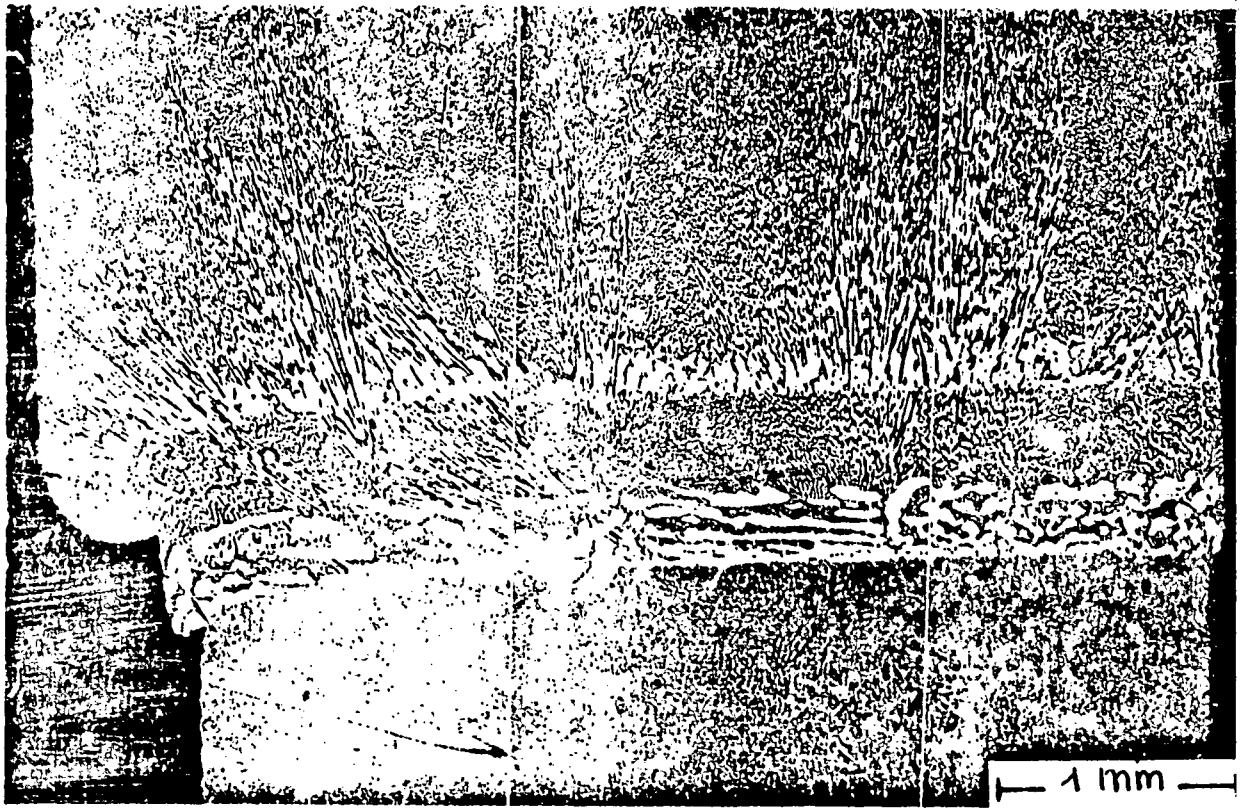

Figure 16-b

Backmelting interface at launch (Z = 14.6/15.3)

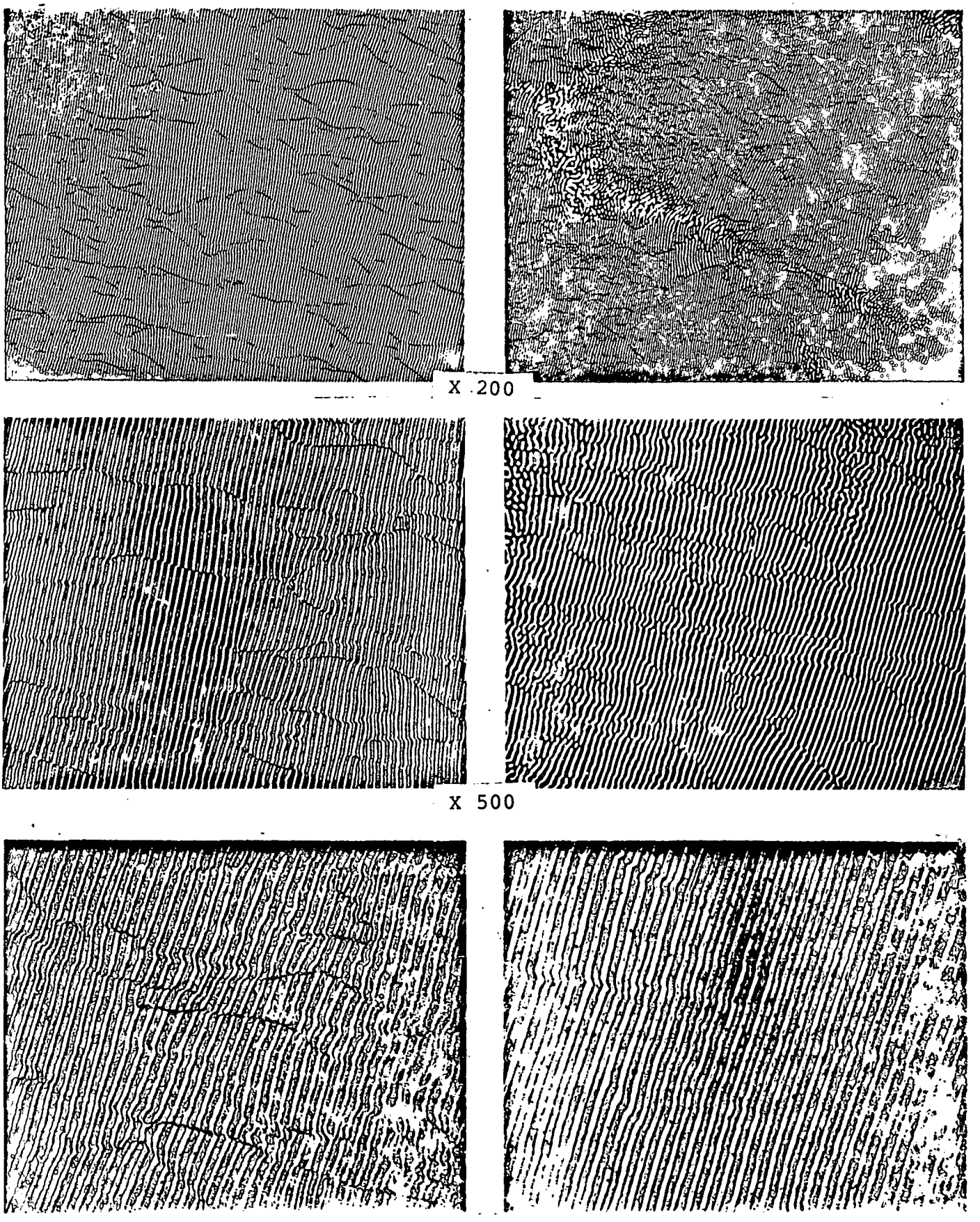

Figure 17
Transversal structure of the eutectic Al_2Cu-Al.

Solidified on ground	Z = 27,9 mm V = 5,2 cm/h	Solidified in microgravity	Z = 27,9 mm V = 7,1 cm/h

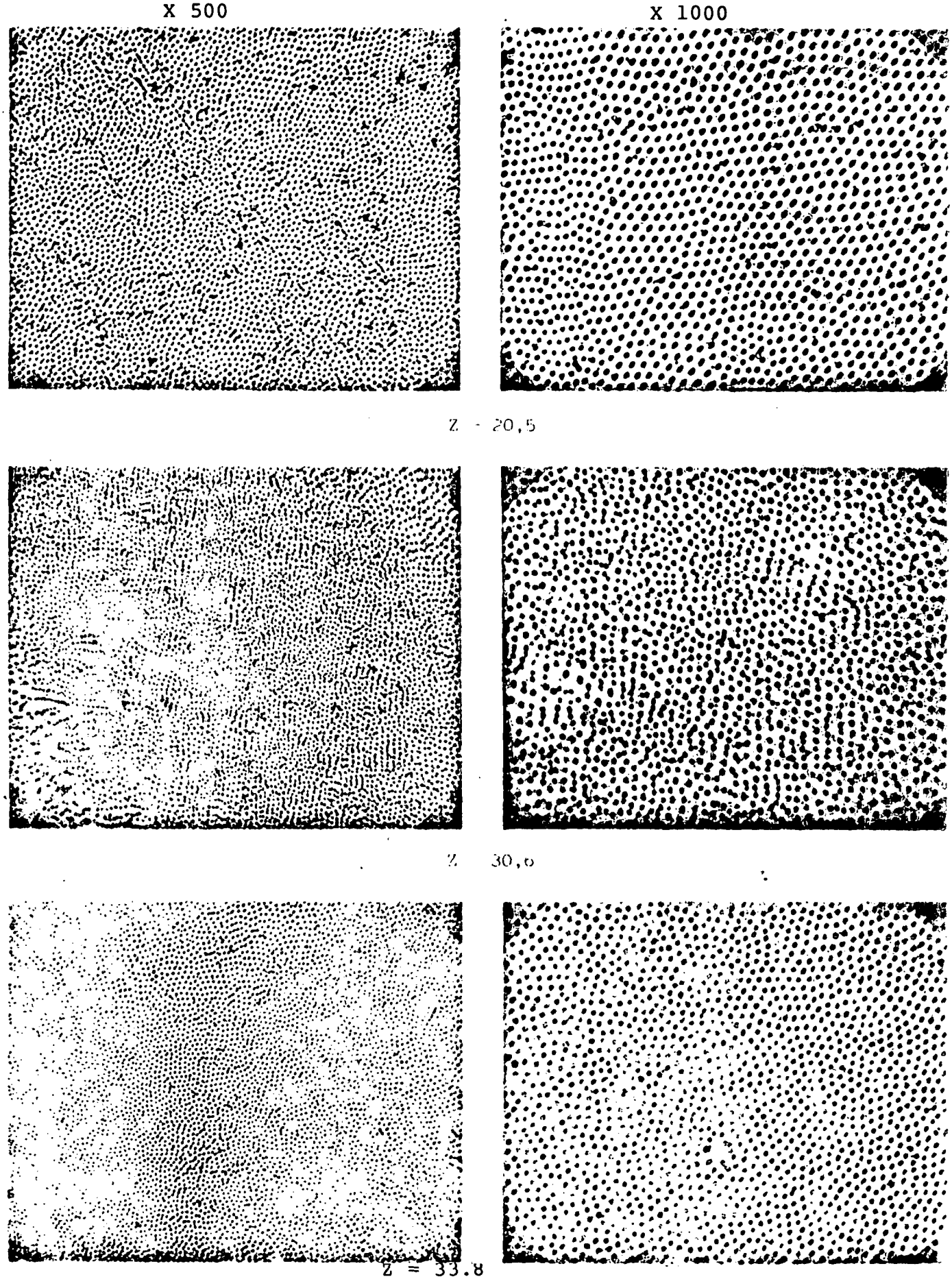

Figure 18
Transversal structure of the eutectic Al_3Ni-Al solidified in microgravity

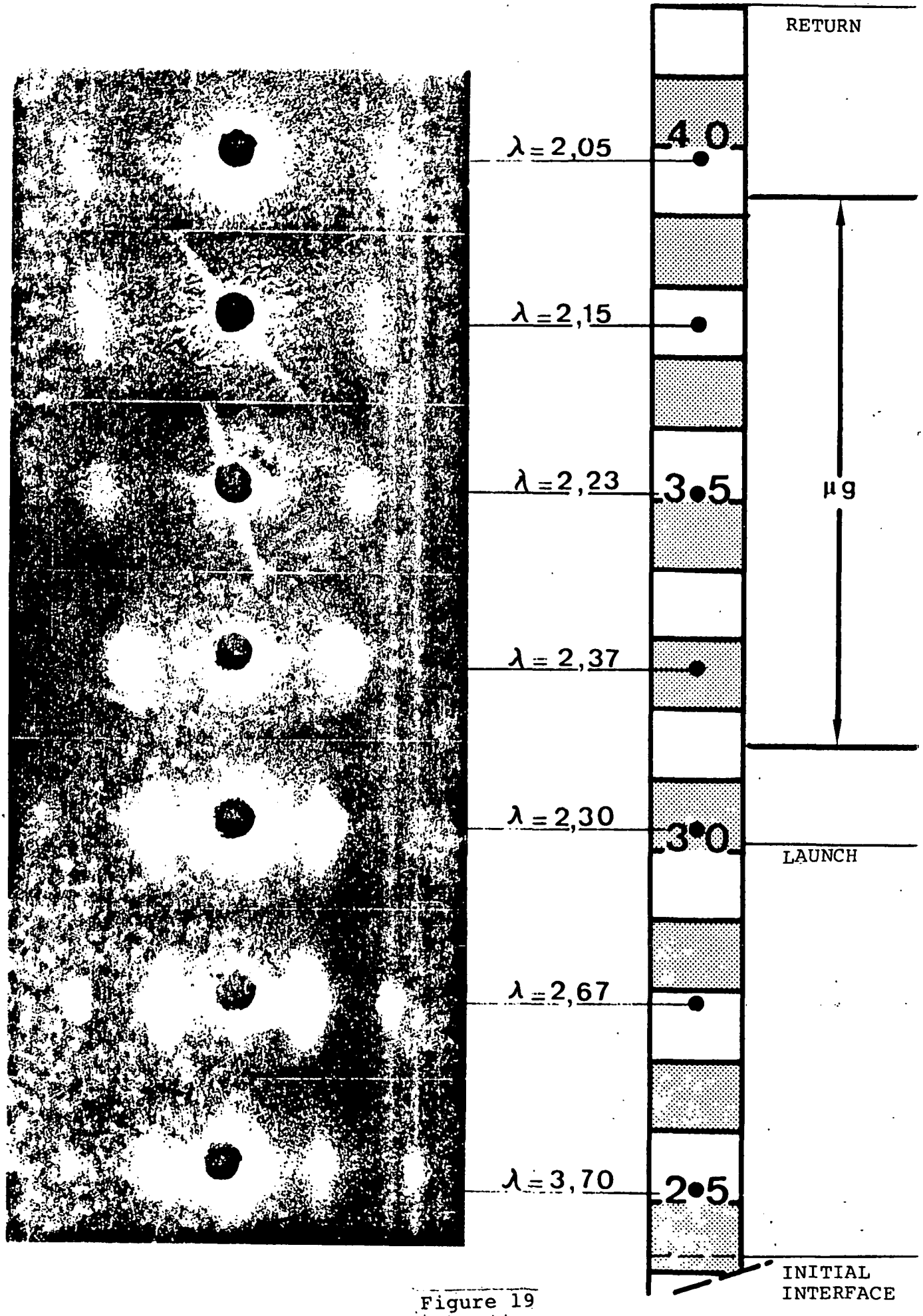

Figure 19

Negatives of laser diffraction on cross-sections of the Al_2Cu-Al sample.

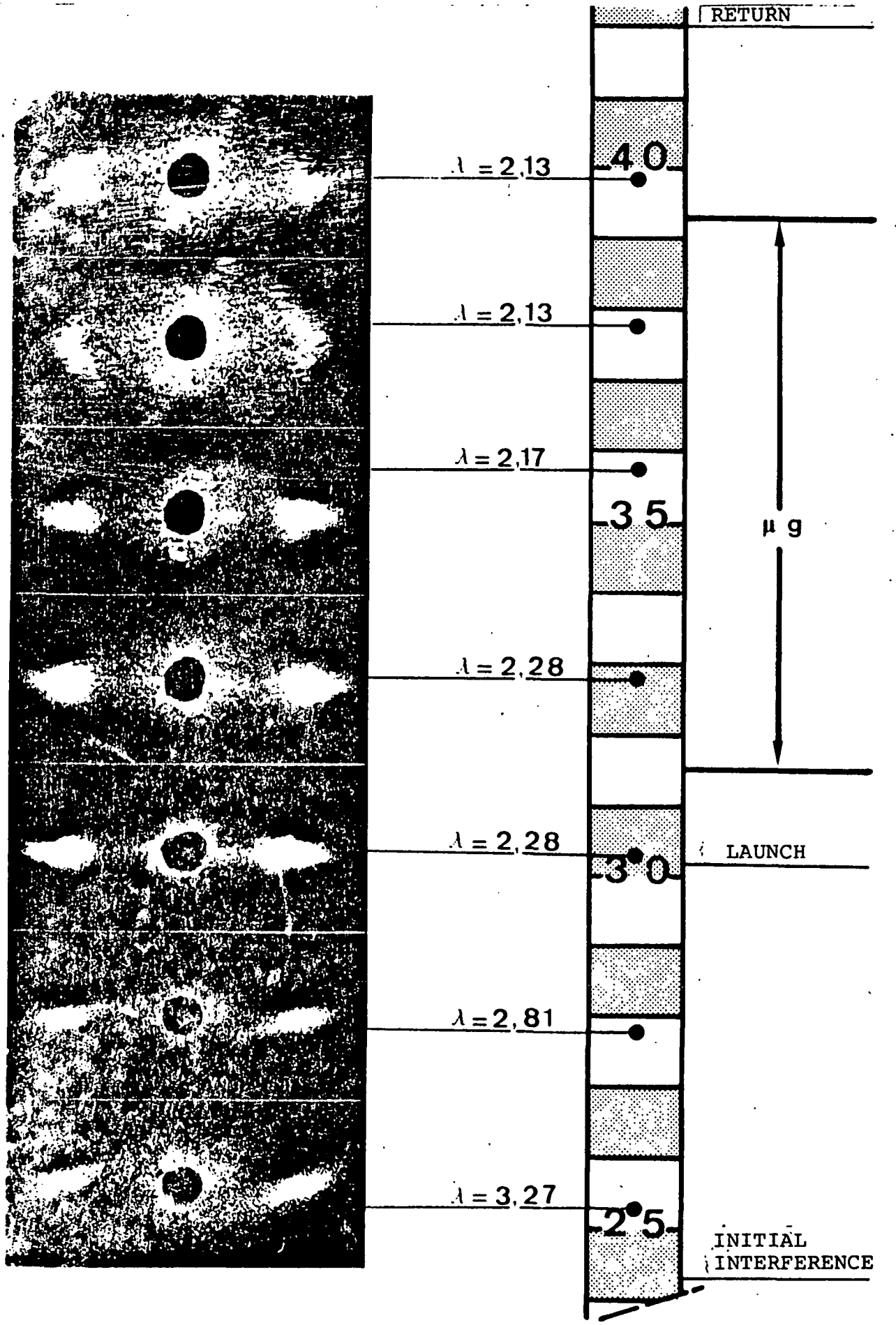

Figure 20

Negatives of laser diffraction on the cross-section of the Al_2Cu-Al sample.

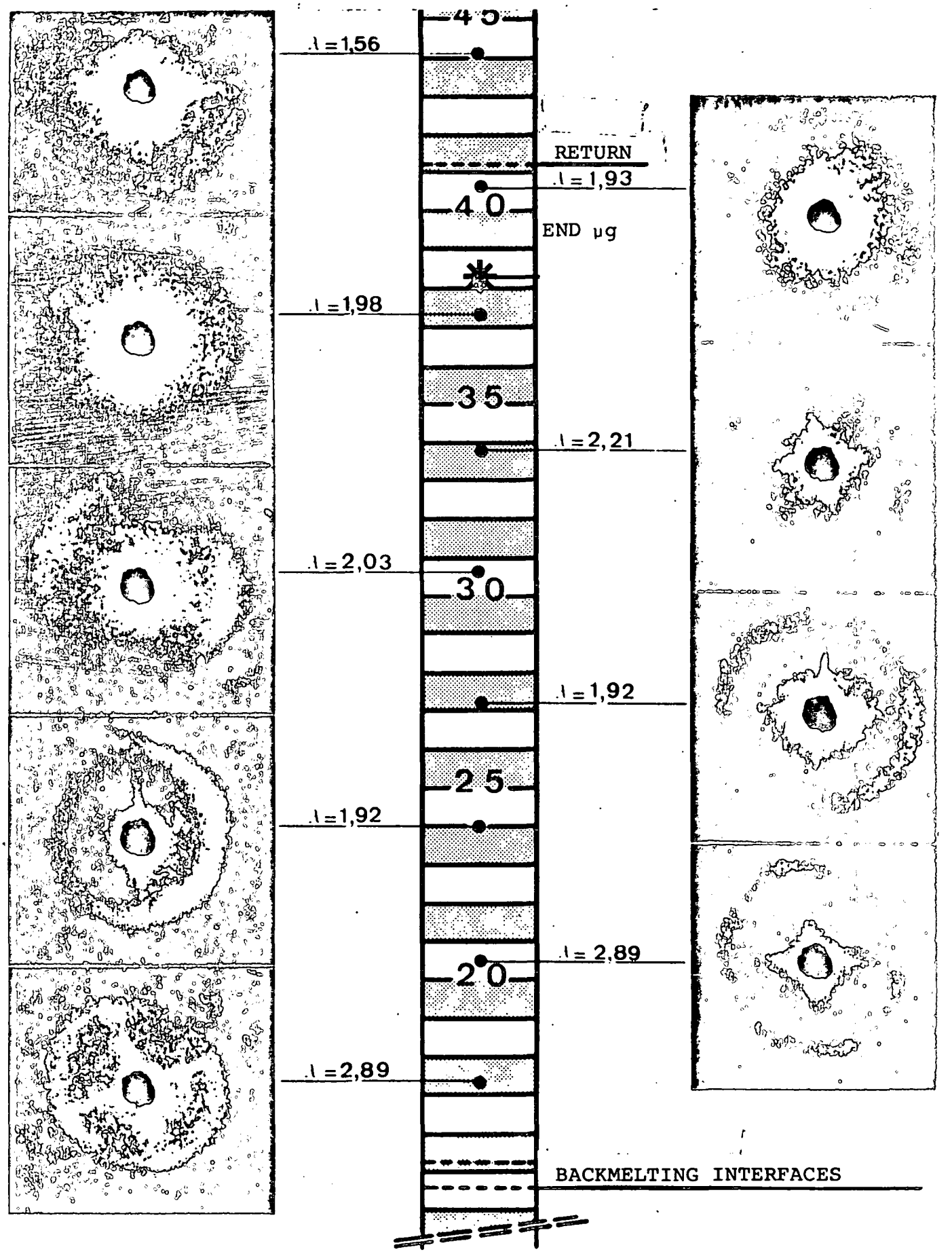

Figure 21

Negatives of laser diffraction on cross-sections of the Al_3Ni-Al sample.

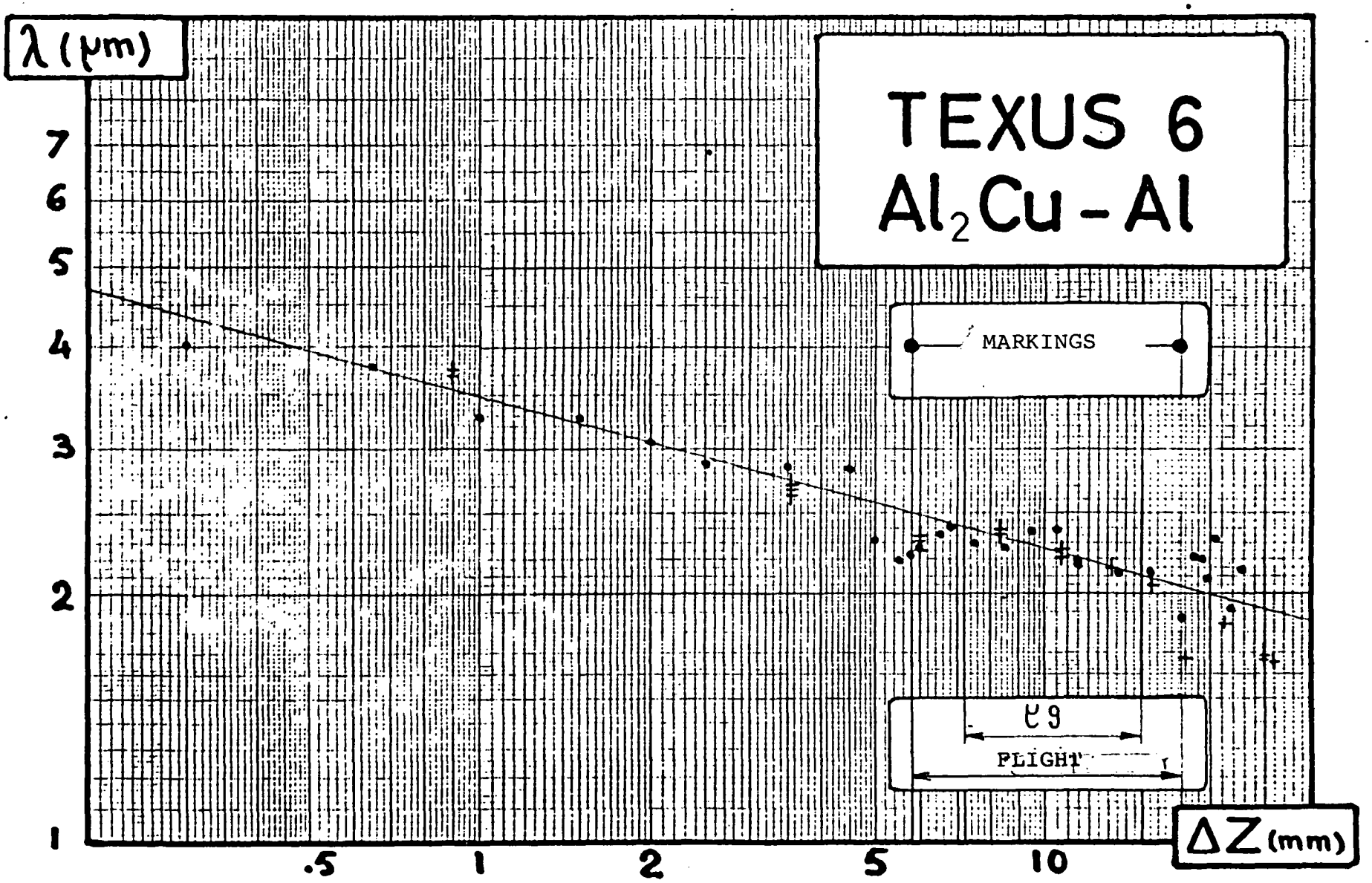

Figure 22
+ Measurements on cross-sections, • measurements on longitudinal sections.

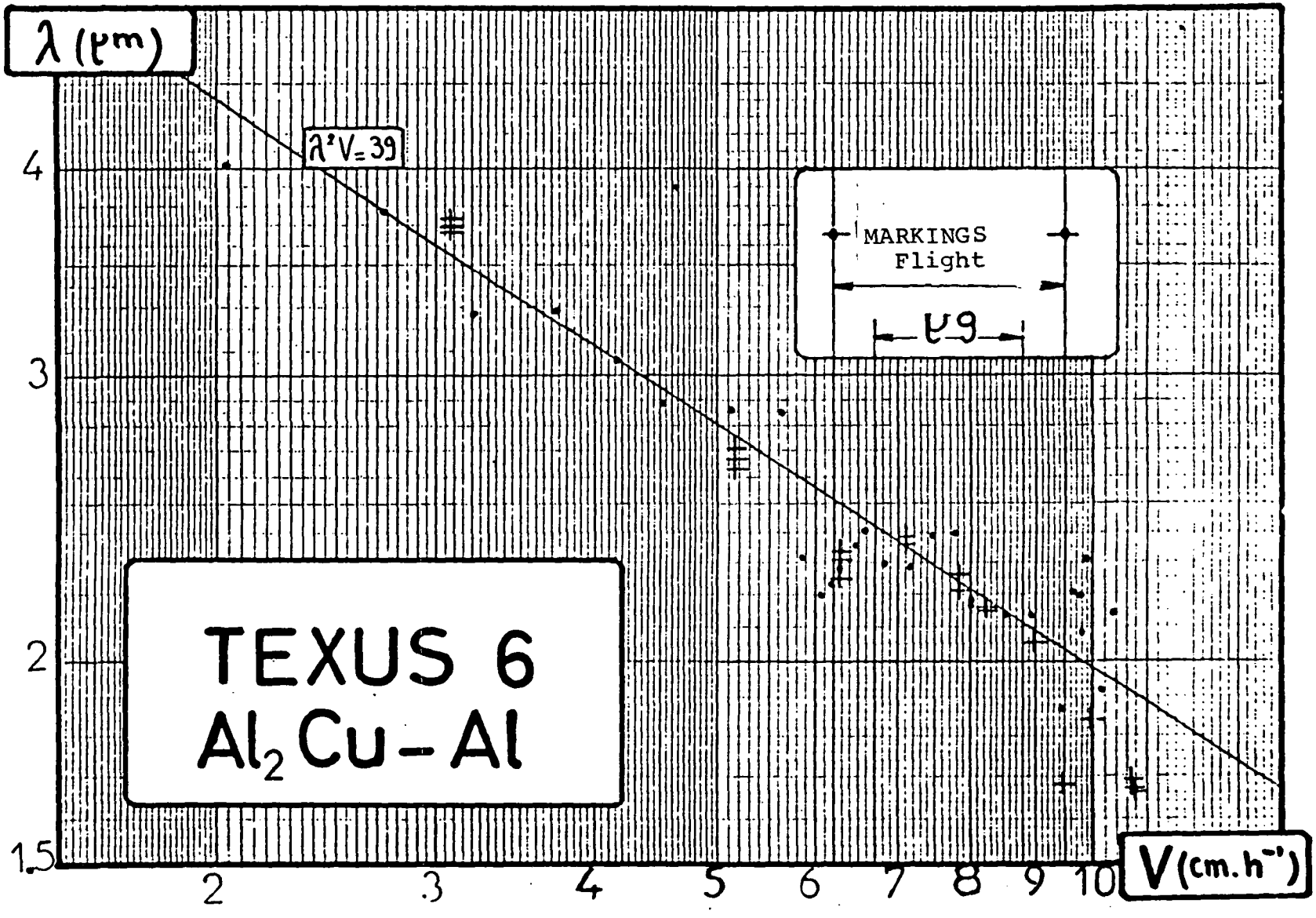

Figure 23

+ Cross-section measurements

• Longitudinal section measurements

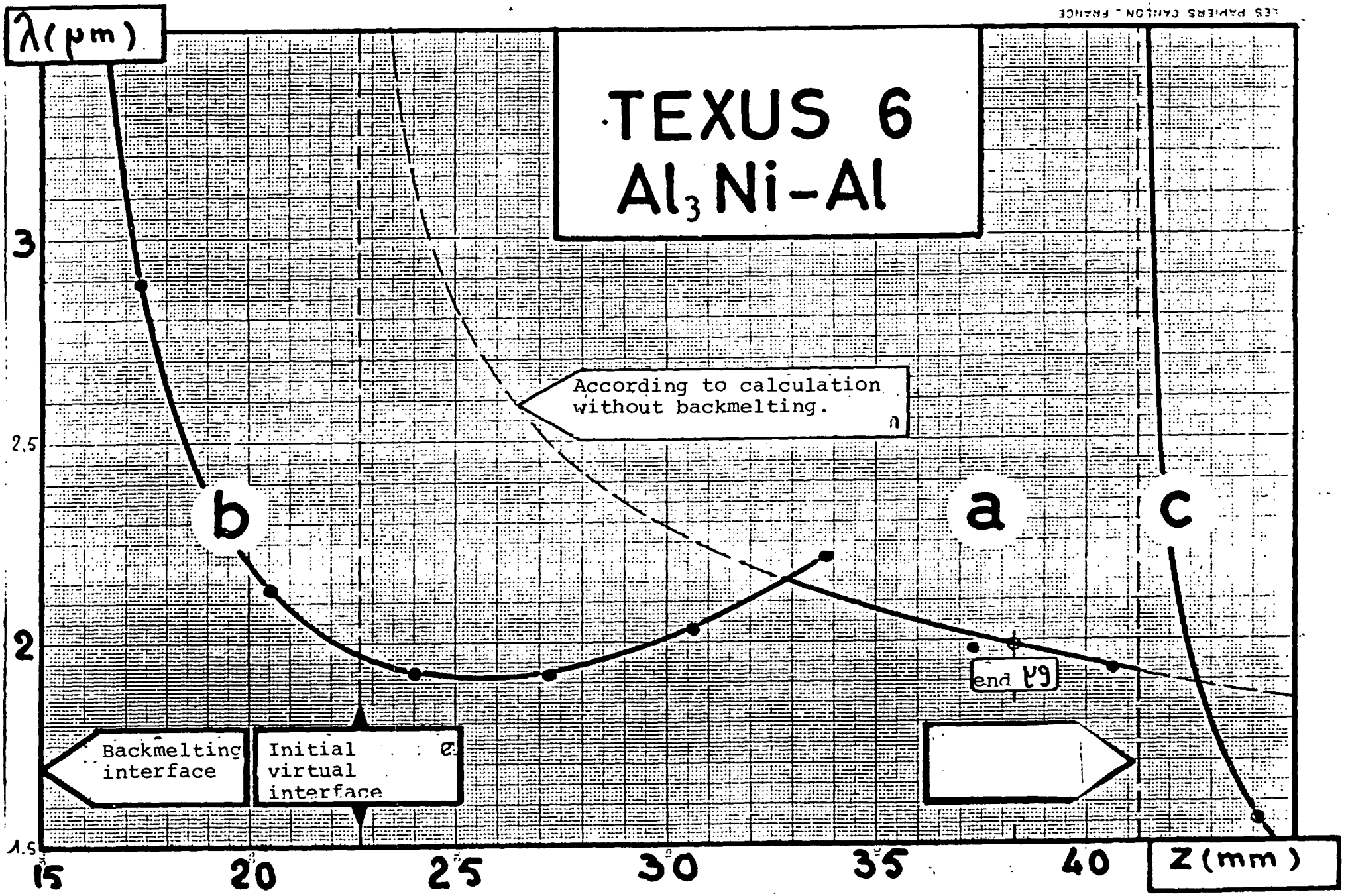
λ(μm)
TEXUS 6
Al3Ni-Al
3
2.5
2
1.5
According to calculation
without backmelting.
b
a
c
end μg
Backmelting
interface
Initial
virtual
interface
15
20
25
30
35
40
Z(mm)

Figure 24

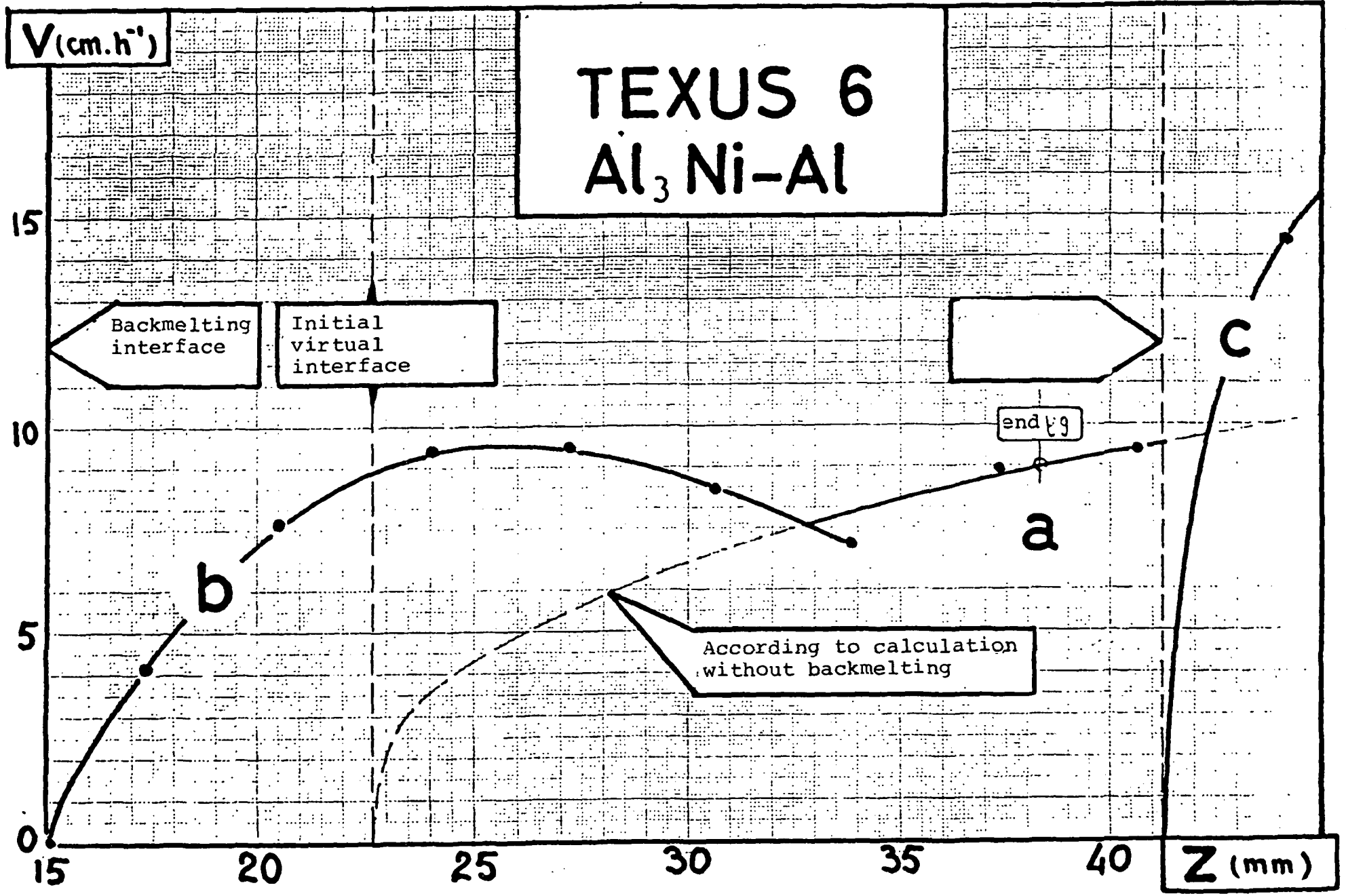
V(cm.h⁻¹)
TEXUS 6
Al3 Ni-Al
Backmelting interface
Initial virtual interface
end
a
b
c
According to calculation without backmelting
0
5
10
15
15
20
25
30
35
40
Z (mm)

Figure 25

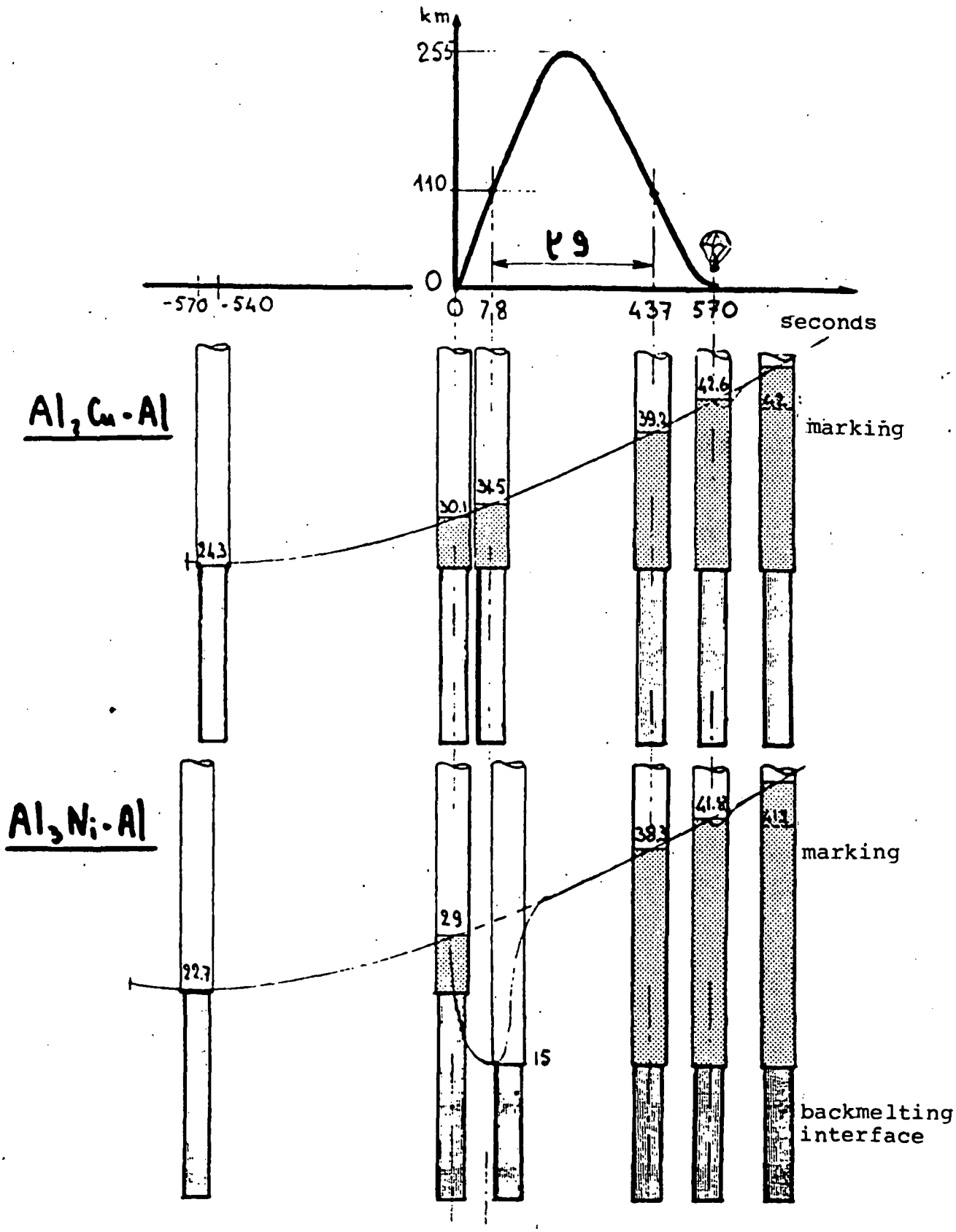

Figure 26
Growth of the eutectic samples during the TEXUS VI mission.